ON HYDROFOILS RUNNING NEAR A FREE SURFACE

S. Schuster and H. Schwanecke
Versuchanstalt für Wasserbau und Shiffbau
Berlin Towing Tank

For the steady state of flow the results of pressure distribution measurements dependent on speed, depth of submergence, angle of attack, and roll angle—both for a flat and for a dihedral hydrofoil—are presented, as well as the results of six-component measurements for two dihedral foils. Below the Froude depth number 1, related to the depth of submergence, the flow and hence the pressure distribution changes according to the shallow water laws; above this figure no significant speed dependency exists. Here the pressure distribution is influenced only by the distance between the hydrofoil and the surface in relation to its profile length. For this situation, which is normal for hydrofoil boats under service conditions, simple theoretical rates for calculating the hydrodynamic forces are given, as well as the results of these calculations in the case of a parallel submerged hydrofoil of great span. By analyzing the separate influences the relation to results of wind tunnel tests can be set up. By means of the results from theoretical and experimental examinations, relations are derived for the vertical and the lateral stability both of flat and dihedral hydrofoils as well as for the influence of sideslip motion.

INTRODUCTION

One of the most important suppositions for the design of hydrofoil boats is the precise knowledge of the flow forces occurring on the foils under given service conditions. There is no doubt that many conceptions are transferable from aerodynamic research but some essential properties like lift distribution and all values of driving performance and running behavior connected herewith will be more or less influenced by the proximity of the water surfaced. During the last twenty years this problem has been treated very often, but further treatment, based on new experiments in the Versuchsanstalt für Wasserbau und Schiffbau (the Berlin Towing Tank), may be expected to clarify and complete the picture. During these examinations the pressure distribution both for completely submerged hydrofoils and for those piercing the water surface, the deformation of the surface, and the flow forces have been measured as well as theoretically treated, all angles being varied.

PRESSURE DISTRIBUTION MEASUREMENT

Two brass hydrofoil models with special borings have been used for measuring the pressure distribution, one of them being a flat hydrofoil and the other a dihedral hydrofoil (V-form), both idealized with circle segment profiles of constant length without distortion (Fig. 1). On the starboard side the flat foil was fitted with 68 borings and the dihedral foil with

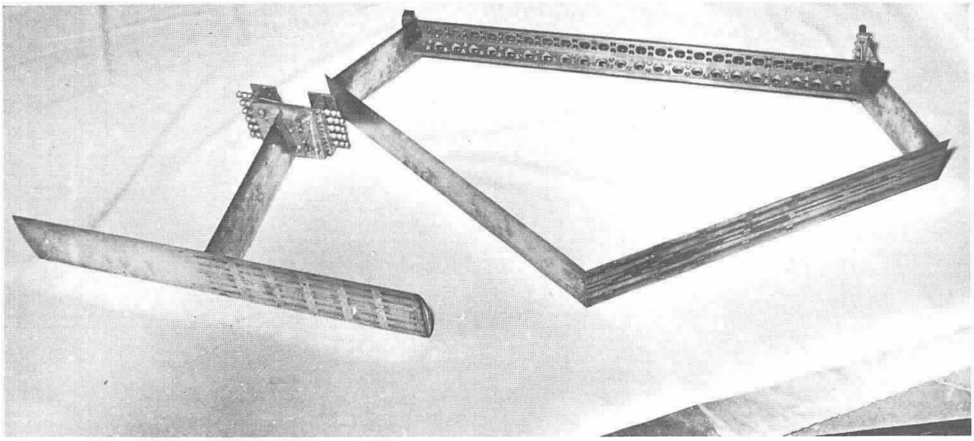

Fig. 1. Hydrofoil models simplified for pressure distribution measurement

49 borings of 1.5-mm diameter. The holes were arranged in sections parallel to the longitudinal axis and connected to each other parallel to the lateral axis. For measurement all the sets of holes but one have been covered with thin plastic strips. Thus, successively, the pressure distribution around the profile for 6 cross sections for the flat foil and 7 cross sections for the dihedral foil has been measured and photographically recorded during each run in the deepwater channel. For the flat foil the angle of attack has been varied from −1 degree to +6 degrees, and the depth of submergence from 30 mm to 240 mm at a speed of $u_0 = 3.7$ m/sec; for a special series the speed was also varied, from 0.4 to 3.7 m/sec. For the dihedral foil the angle of attack has been kept constant at +1 degree while the rolling angle has been varied from 0 to 33 degrees, one arm of the hydrofoil being parallel to the water surface when the rolling angle was 33 degrees. The measured pressure in relation to the ram pressure has been plotted versus the profile length for every section. Integration of the pressure curves results in the local lift coefficients, which in turn by integration over the span supply the total coefficient. For checking these values and for finding the drag three component tests have been made.

Flat Foil

The variation with speed for the flat foil first of all confirmed the shallow water effect as found by Laitone [1], Parkin, Perry, and Wu [2] and Plesset and Parkin [3], which occurs especially at the critical speed $u_0 = \sqrt{gh}$ (Fig. 2), where h denotes the distance between the trailing edge and the undisturbed water surface.* At a speed sufficiently above this value the ratio between depth of submergence and length of profile only is authoritative for the course of the pressure curve. Samples are shown in Figs. 3 and 4. Herein the characteristics of the diagrams versus h/c and α are different. The local lift coefficients indeed change in the same sense as depth of submergence and angle of attack, but in the first case the pressure distribution is unchanged, while it is varying much in the second case. Therefore, approaching the surface cannot be substituted by a reduction of the angle of attack.

*A nomenclature list is given at the end of the paper.

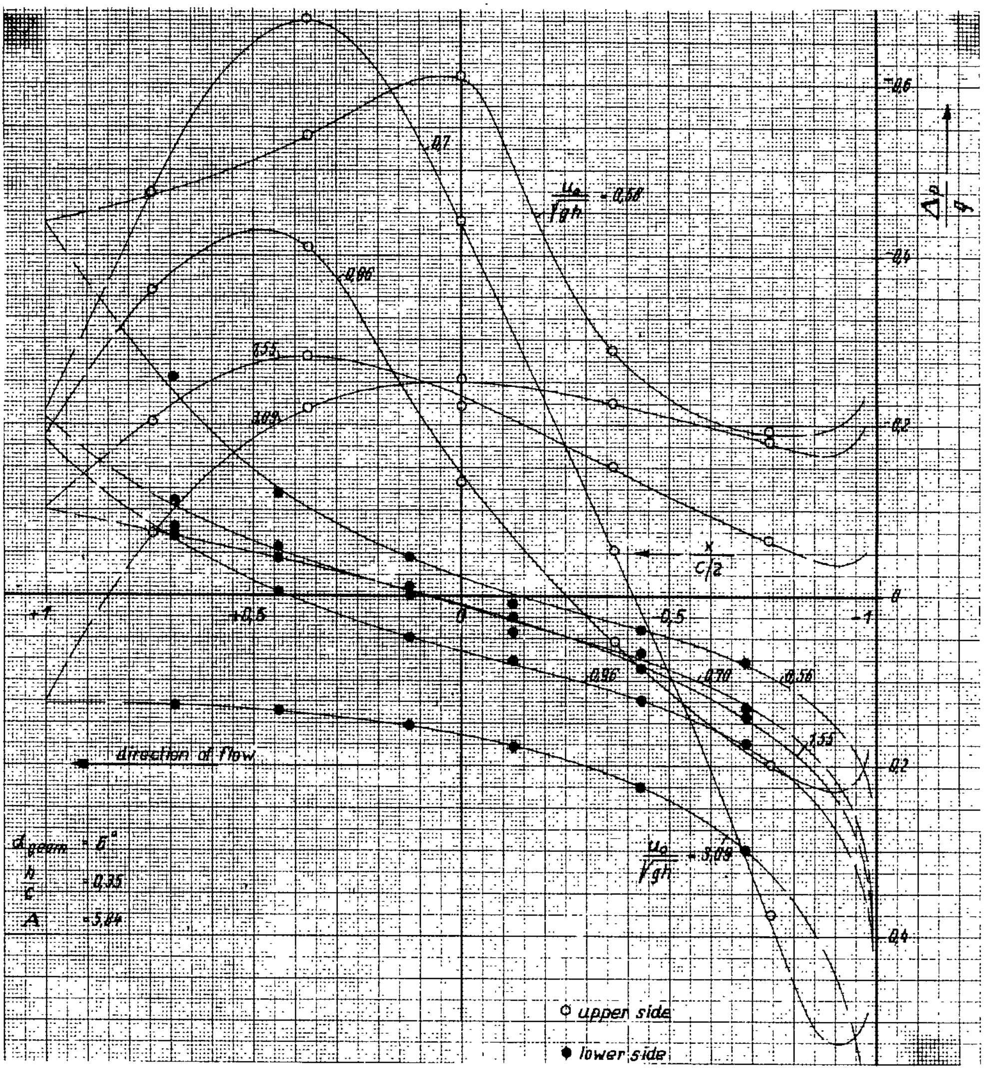

Fig. 2. Pressure data for the flat foil of circle segment profile at subcritical and supercritical velocity

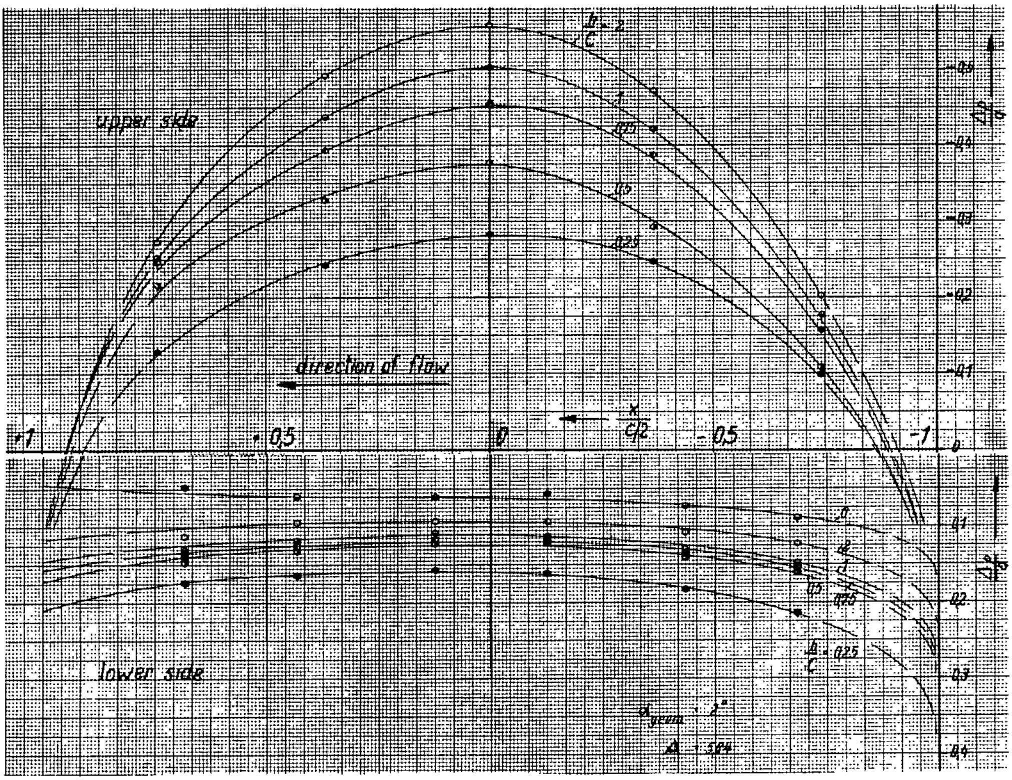

Fig. 3. Pressure distribution for $\alpha = 2$ degrees and varying h/c ratios for the flat foil

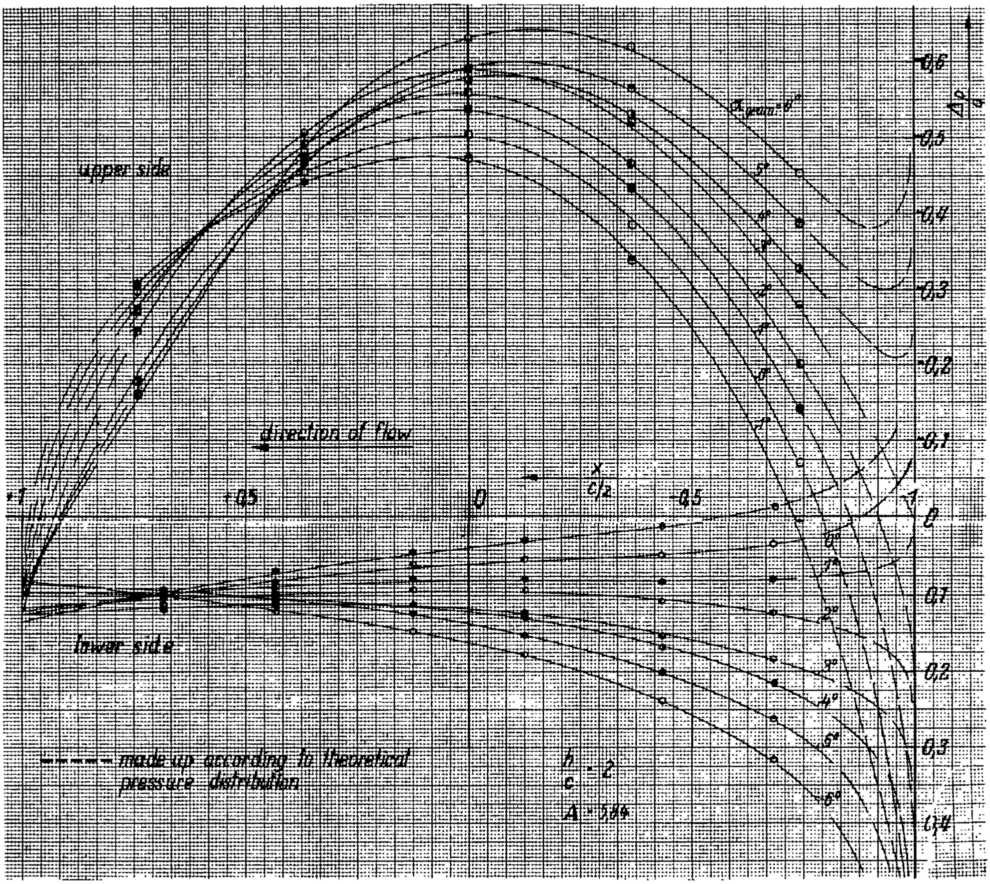

Fig. 4. Pressure distribution for $h/c = 2$ and varying angles of attack for the flat foil

The lift distribution over the span can be seen in Fig. 5, the lift coefficients for the complete hydrofoil are shown in Fig. 6, and the components of the suction side as well as those of the pressure side and the ratio between these components are shown in Figs. 7 to 9, where the C_L values are related to conditions in great depth (infinite medium). In approaching the water surface the lift of the foil running at supercritical speed decreases nearly along a parabola with the depth of submergence, especially for $h/c < 2$, the effect of the suction side being diminished and the effect of the pressure side being augmented. This change will decrease for increasing angles of attack. It is remarkable that the drag coefficient is decreasing with the decrease of depth in spite of the increasing waves (Fig. 10).

Summing up, the results of these tests with the flat foil were as follows:

1. Owing to the proximity of the water surface an additional velocity is induced which is contrary to the direction of flow. This results in an increase of the lift component on the pressure side and in a decrease on the suction side. Due to the suction side's greater part of the total lift in the deep submerged position, a diminution of lift thus results. Owing to the minor flow velocities at both sides the profile resistance decreases.

2. Owing to the curvature of flow along the upper side the effective profile curvature is diminished. Thus the angle of zero lift will be shifted toward positive values, and the effective angle of attack and thereby the lift coefficient will become less. Relatively this influence decreases with increasing angle of attack.

3. Owing to the continual lift diminution in the range $2 > \bar{h} > 0$ a submergence stabilizing seems to be possible even for hydrofoils not piercing the water surface.

Dihedral Foil

The measured lift distribution for the dihedral foil can be seen in Fig. 11. The pressure distribution over the profile is similar to that for the flat, fully-submerged hydrofoil. The joint of the two foil halves at the keel point, as well as that between foil and struts, causes an increase of lift on the suction side, and in the first case simultaneously decreases the pressure at the lower side. When piercing the surface a diminution of the local lift occurs within the region of the surface approach in such a manner as though the results of flat parallel submerged foils had been transferred stripwise.

Figure 12 shows the lift decrease of both foils plotted versus the relative submergence. This diagram shows also the test results of Land [4], which were found at substantially higher speeds.

The lift diminution for the complete dihedral hydrofoil caused by the surface effect can be found by integration of the local values

$$C_L/C_{L\infty}$$

within the range of $\bar{h} = 0$ to $\bar{h} = \bar{h}_{\text{keel}}$. The mean of $(\overline{C_L/C_{L\infty}})$ amounts to approximately 0.5 for $\bar{h}_{\text{keel}} = 0.5$, to 0.8 for $\bar{h}_{\text{keel}} = 1.5$, and to 0.9 for $\bar{h}_{\text{keel}} = 5$.

Summing up, it follows from the tests with the dihedral hydrofoil that:

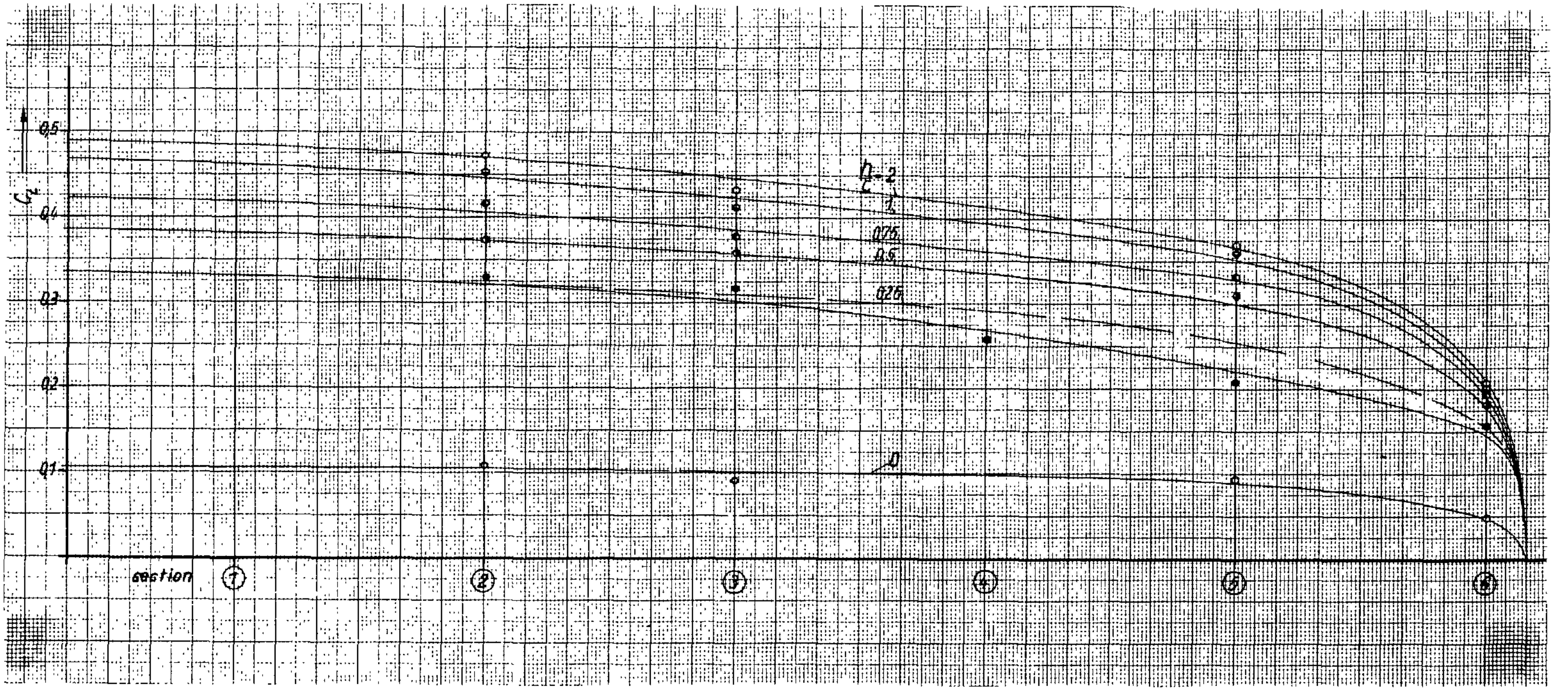

Fig. 5. Lift distribution over the span of the flat foil for varying h/c ratios

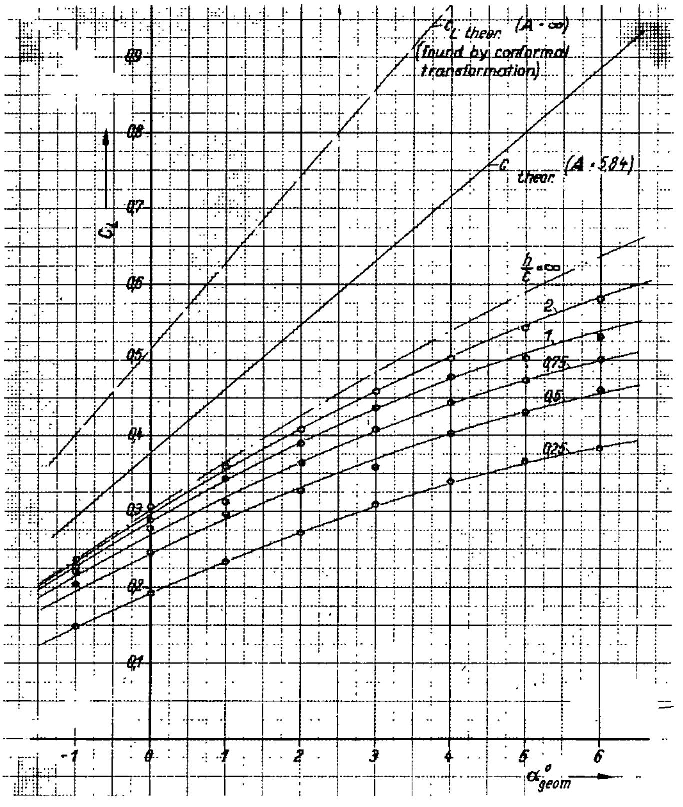

Fig. 6. Lift coefficients of the flat foil

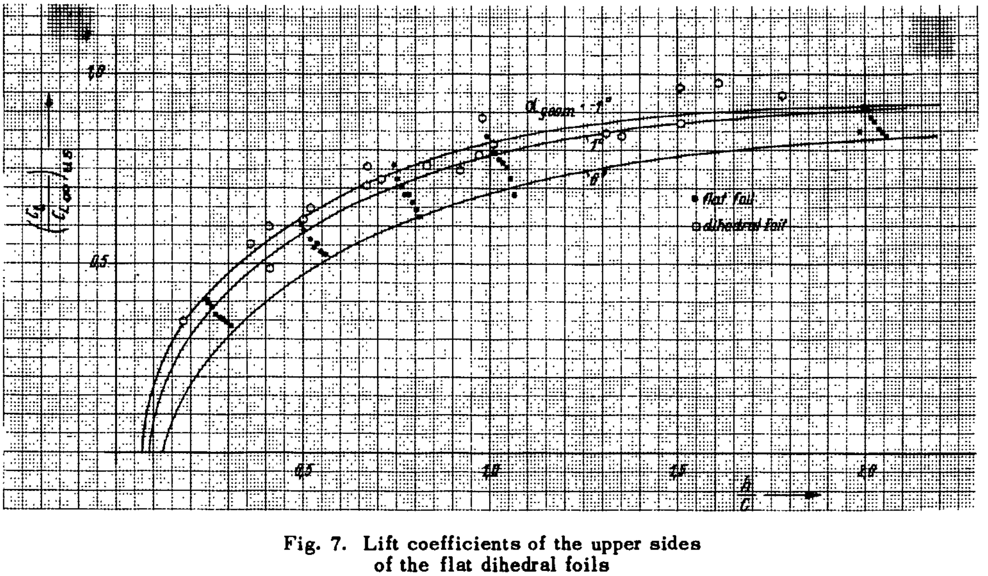

Fig. 7. Lift coefficients of the upper sides of the flat dihedral foils

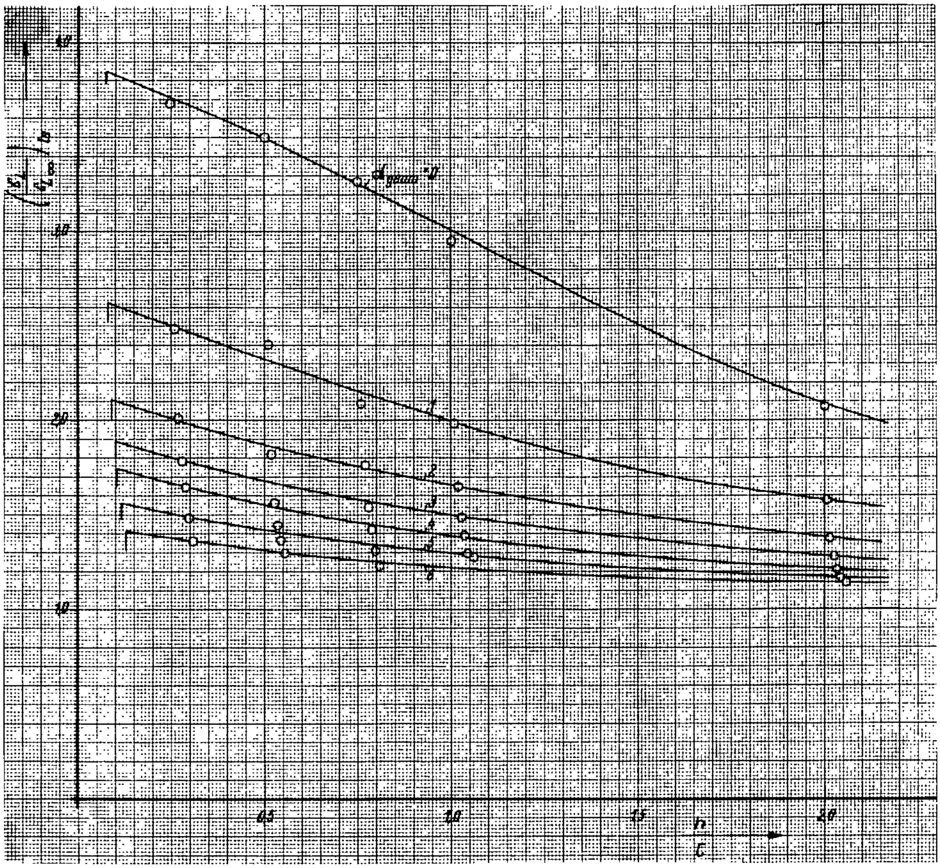

Fig. 8. Lift coefficients of the lower side of the flat foil

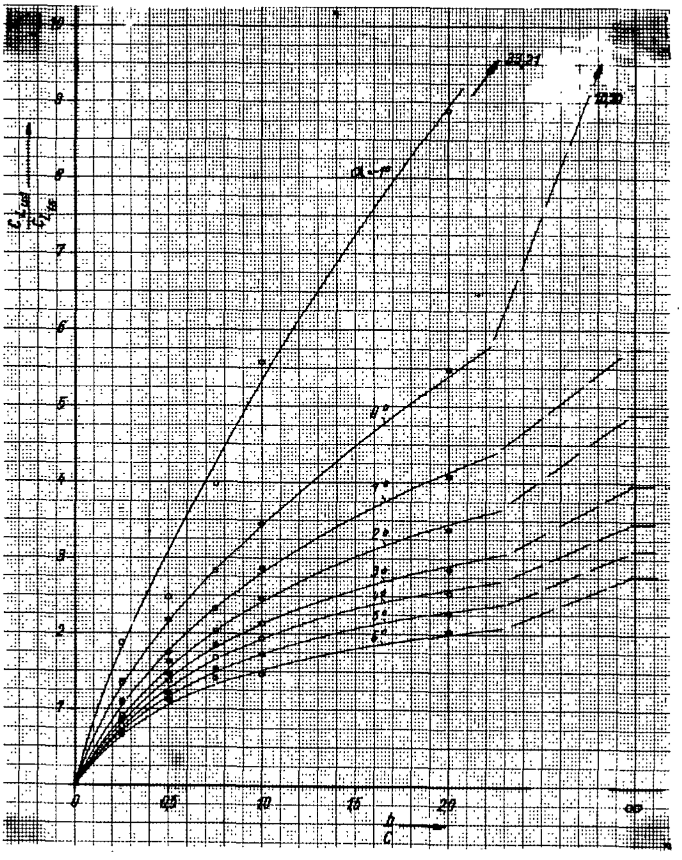

Fig. 9. Relation between lift of the upper side and the lower side of the flat foil

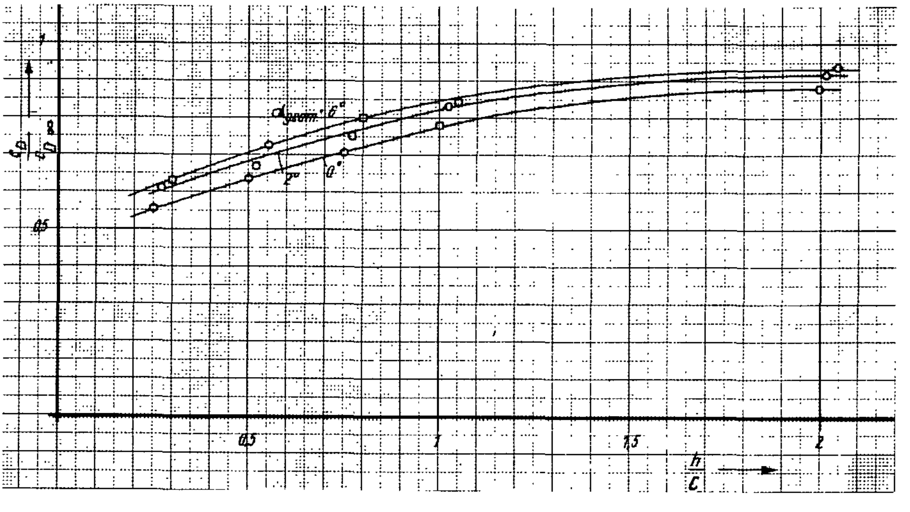

Fig. 10. Drag coefficients of the flat foil

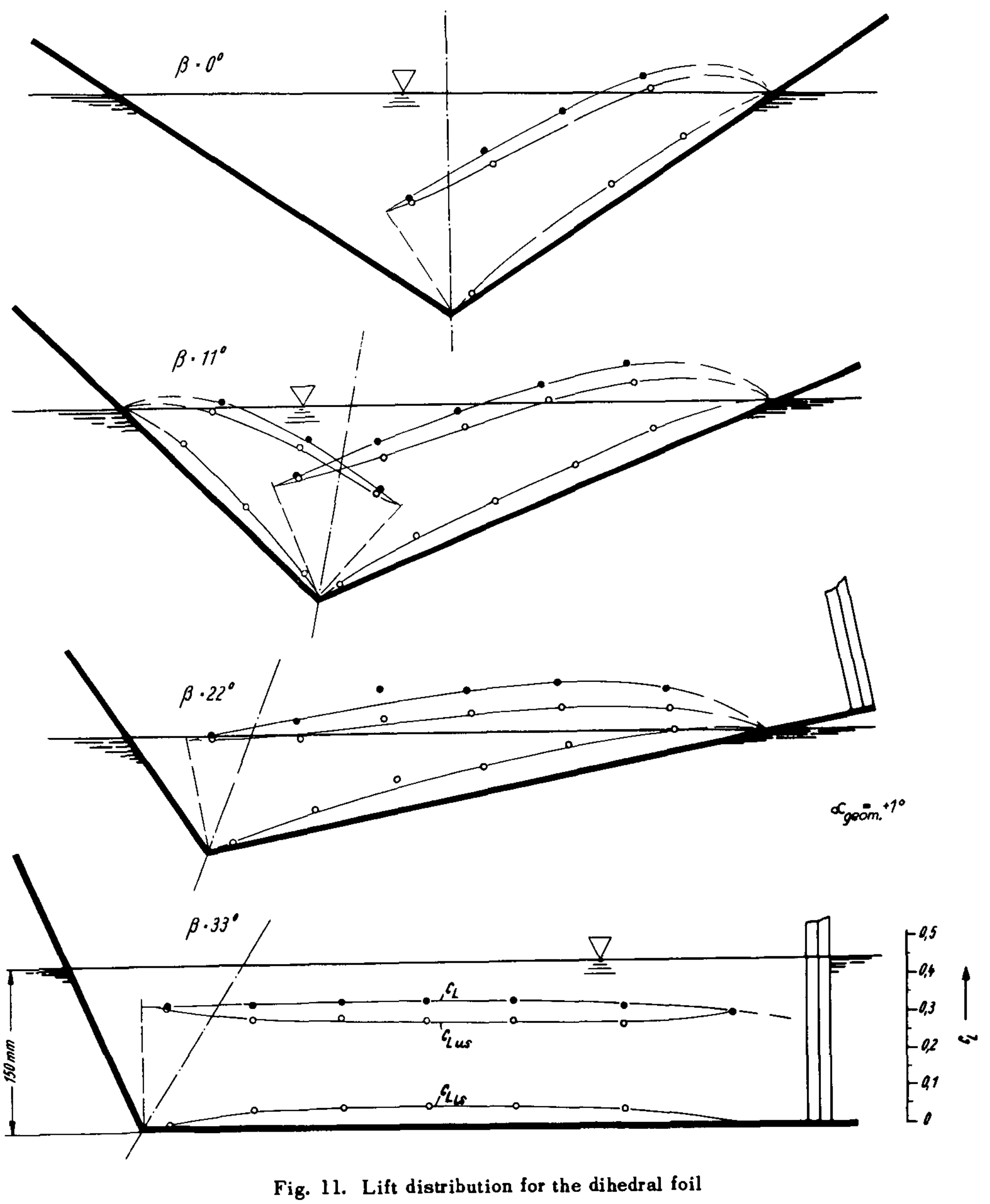

Fig. 11. Lift distribution for the dihedral foil

646551 O—62——12

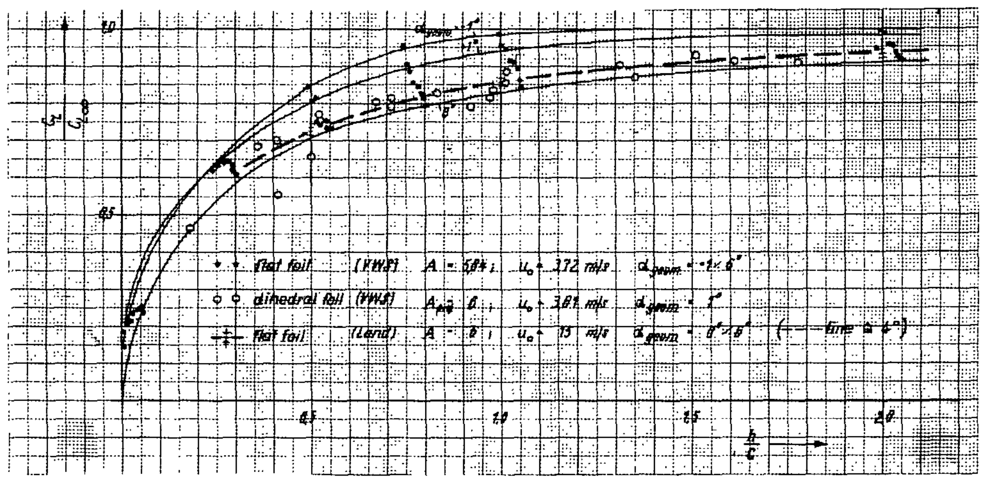

Fig. 12. Comparison of lift coefficients versus relative depth

1. The test results of fully submerged flat foils can be transferred to emerging foils by means of the strip method. The lift decrease toward the outer regions becomes also measurable for $h/c < 2$ and essential for $h/c < 1$. Enlarging the profile length in the outer regions therefore seems to be less practical since the h/c value will be smaller and the influence of the water surface will be extended to larger regions of the span. According to item 2 in the summing up for the preceding subsection, it would be better to increase the angle of attack, i.e., to distort the foil.

2. Since the strip method can be used for the rolling dihedral hydrofoil too, there is no special need for investigating the influence of the roll angle. Even for hydrofoils in a sideslip motion the measurement of the pressure distribution can be retained, for in this case only the local angles of attack are changed, the influence of which has been determined for the flat parallel submerged foil.

STATE OF FLOW EXAMINATION

If the existence of a shallow water effect could be concluded from the pressure measurement, then the transition from the subcritical to the supercritical range of the Froude depth number must be perceptible by a change of the surface deformation. Tests with a flat parallel submerged hydrofoil, extending sideways to the walls of a circulating water channel, proved that there is indeed a transition from a steady flow to a rapid flow with a hydraulic jump between. With regard to the speed increment above the foil and to the slope of the water surface connected herewith, a local Froude depth number

$$F_{h'} = \frac{u_0}{\sqrt{gh'}} \left(1 + \frac{\pi}{2}\alpha\right)^{3/2}$$

where h' denotes the minimum depth above the foil, can be defined as a barrier. The deformation corresponds to pictures shown in the publication of Parkin, Perry, and Wu [2].

Below $F_h' = 1$, i.e., in the subcritical speed range, the depth of submergence of any foil plays a similar part for the circulation as the water depth does for the orbital velocity of waves in shallow water. Thus correspond the C_L reduction on the upper side and the wave speed reduction

$$\frac{C_{Lh}}{C_{L\infty}} \hat{=} \frac{u_h}{u_\infty} = \sqrt{\tanh \frac{gh}{u_\infty^2}} \hat{=} \sqrt{\tanh \frac{(C_L/C_{L\infty})^2}{F_h^2}} .$$

Hence

$$F_h^2 = \left(\frac{C_L}{C_{L\infty}}\right)^2 \Big/ \tanh^{-1} \left(\frac{C_L}{C_{L\infty}}\right)^2$$

follows.

To be sure, this can be seen exactly only at small depths, for example for $h/c = 0.37$ as in Fig. 13. For larger depths the transition is smoothed at $F_h = 1$ and disappears gradually in the same manner as it does in deep water. Above $F_h = 2$ no dependency of the Froude depth number exists. Hydrofoil boats generally run by dynamic lift at a speed more than 25 knots and at a submergence less than 2 m. This corresponds to a smallest Froude depth number of about 3.

Summing up, the results of examination of the state of flow are as follows:

1. The hydrofoil is susceptible to the shallow water effect. For operating conditions of hydrofoil boats the flow pattern is a supercritical one. For theoretical considerations by analogy from wave theory, rapid flow is presumed in the direct neighborhood of the hydrofoil in place of orbital motion for waves.

2. For individual hydrofoils no critical speed barrier can exist as it does for displacement ships in shallow water, given by speed and depth. But for the complete craft fitted with several hydrofoils such a barrier, of course, can exist, since the wave formation behind the hydraulic jump follows the Froude depth number given by the water depth and changes the flow against the next hydrofoil in line.

3. The only significant quantity for the influence of the water surface on the circulation around a hydrofoil in the supercritical range is the relative depth of submergence of the foil element, $\bar{h} = h/c$. It is independent of the configuration and speed of the hydrofoil.

FLOW FORCES MEASUREMENT

In 1941 six component tests on hydrofoils already had been made in the circulating water tunnel of the firm Gebr. Sachsenberg AG., Berlin, under the direction of G. Weinblum. The results were published at that time only for a restricted number of persons.

In one case a model of a dihedral foil with a constant circle segment profile of a constant length $\ell = 96$ mm and a thickness $t = 6.4$ mm was used [6]. The dihedral angle could

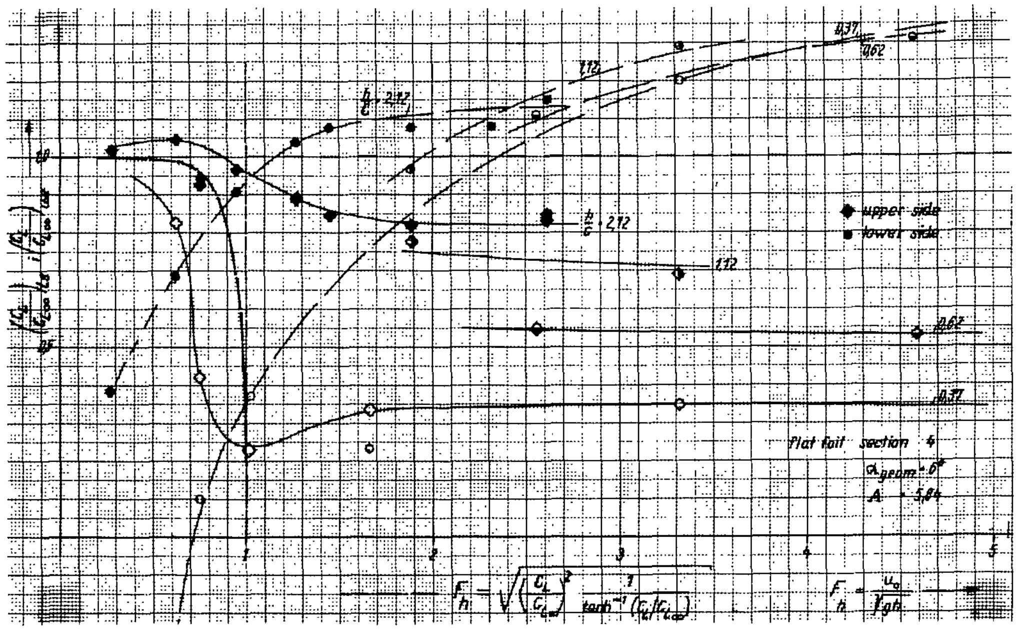

Fig. 13. Local lift coefficients of the upper and lower sides of the flat foil for different h/c ratios

be changed between 15 degrees and 50 degrees. Variations of span from 200 to 600 mm, of roll angle from 0 to 10 degrees, and of angle of attack from –5 to +7 degrees were made. All the values of C_L, C_D, and C_{M_x} were measured for a constant speed of 4 m/sec. For example such diagrams could be drawn as can be seen in Figs. 14 and 15 for lift and drag, or in Figs. 16 and 17 for the roll moment. The results for the mean span of 400 mm were $C_{L_{max}} = 0.36$, $dC_L/d\alpha = 2.72$ to 3.14 related to the effective angle of attack, $\alpha(C_L = 0) = -4.5$ degrees, $C_{D_{min}} = 0.015$, and $\varepsilon_{min} = 0.07$.

A comparison of the results for the different variations showed with regard to lift, drag, drag-lift ratio, and lateral stability:

1. The aspect ratio $A = b^2/F$ possibly should be chosen not less than 4. Raising it beyond 5 will give but little additional profit.

2. As long as the proximity of the surface does not influence the complete foil, i.e., as long as $\bar{h}_{max} > 1$, the $dC_{m_x}/d\alpha$ value will increase for decreasing dihedral angles, for $\bar{h}_{max} < 1$ the ratio diminishes rapidly. For the aspect ratio 4.15 the maximum relative depth is 1 for a dihedral angle of 27 degrees. The optimal dihedral angle for this aspect ratio is around 30 degrees.

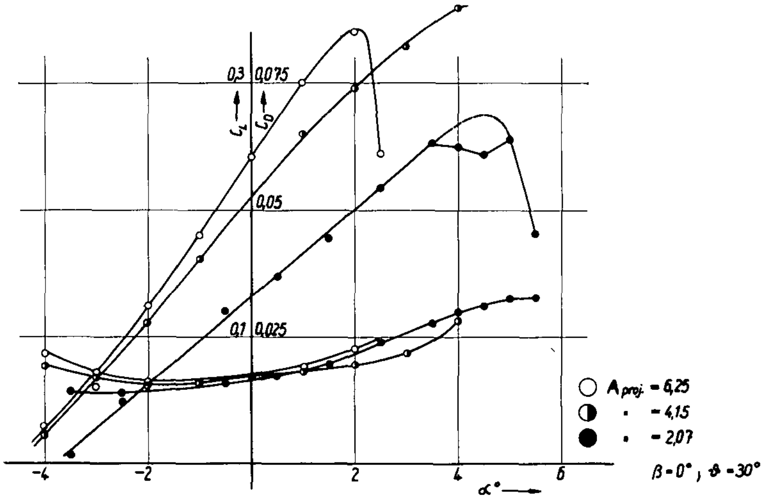

Fig. 14. Influence of the aspect ratio on the lift coefficients (upper curves) and drag coefficients (lower curves) of a dihedral foil

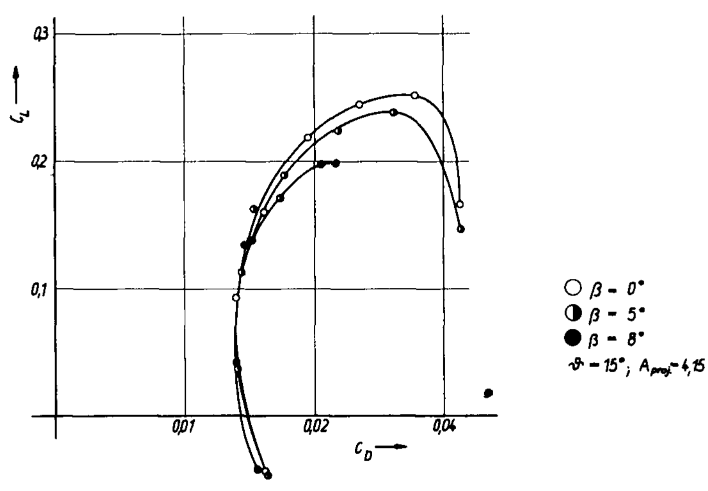

Fig. 15. Influence of the rolling angle on a dihedral foil

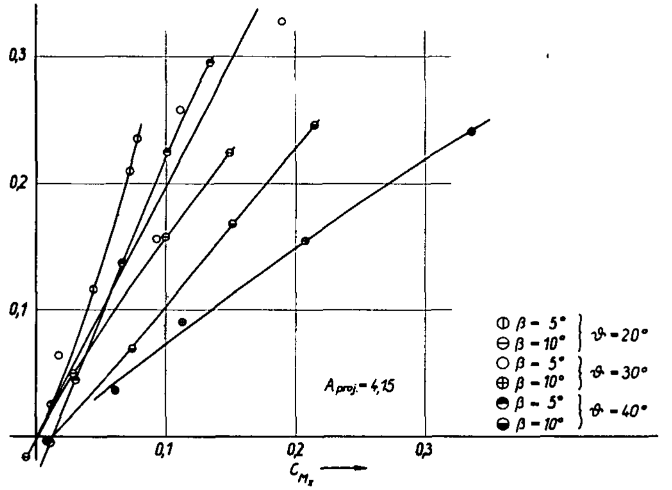

Fig. 16. Influence of the dihedral and rolling angles on the rolling moment

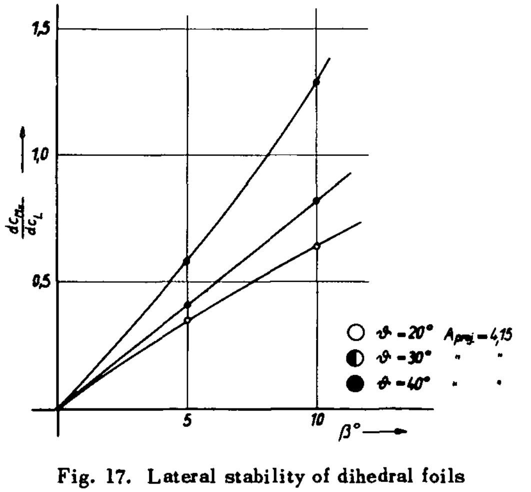

Fig. 17. Lateral stability of dihedral foils

3. By rolling, the flow, being symmetrical before, becomes nonsymmetrical. When the span is kept equal the aspect ratio and the angle of inclination between foil and water surface increase for one part as much as they decrease for the other. Indeed rolling has the same effect as superposing the influences of aspect ratio and dihedral angle. At small roll angles C_L and C_D are only slightly changed. At greater angles lift and ascent of lift drop more and more and the resistance increases.

The results of this first test series were complemented in 1958 by six component measurements in the circulating water tunnel of the VWS [7]. The dihedral hydrofoil model already described for the measurements of the pressure distribution with a fixed dihedral angle $\vartheta = 33$ degrees was used. The flow speed was about 2 m/sec. The influence of rolling and sideslipping in particular were examined.

First of all Fig. 18 shows the geometrical variation of the effective angle of attack of the pressure-side chord along with the roll angle and with the sideslip angle. For instance if such a hydrofoil is running straight-on with $\alpha = 1$ degree, then for the profiles, 0.8 degree is the effective angle. If there does exist a sideslip angle of $\gamma = 10$ degrees toward starboard – for instance when turning to port – the effective angle of attack will increase on the starboard side to +6 degrees while on the port side it will decrease to –4 degrees. If there is an additional roll angle of about $\beta = +20$ degrees toward the center of the turning circle, then this angle of attack difference will be increased to +8 degrees and –7 degrees respectively. For a rolling angle of $\beta = -20$ degrees to the outside, a diminution of the effective angles of attack to +2.5 degrees and –1.5 degrees respectively will result. An augmentation of the sideslip angle causes a nearly linear augmentation of these angles of attack.

Since therefore for hydrofoil boats under service conditions the angle of attack can spread over a very wide range, the course of the coefficients for lift, drag, and pitching moment has been measured for a 45-degree variation of the angle of attack (Fig. 19). Here the flow separated at about +8 degrees on the upper side and at about –10 degrees on the lower side. The lift coefficient will increase, of course, after such a sudden breakdown but the drag-lift ratio $\varepsilon = C_D/C_L$ then will be three times as high as it was before (Fig. 20). The fact that relatively high negative lift values can be obtained is of no importance for practice. In turning circles for the inner side, i.e., on the port side when turning to port, a decrease of lift may, of course, be desired, even down to zero. But it should not reach negative values, since an adequate raising of lift on the outer side beyond twice the value as before seems to be unlikely considering the augmentation of drag, the diminution of speed, and the smaller submerged area of the outer foil, which is reduced by rolling. For running with a following sea – a situation when negative angles of attack will occur easily – such a negative lift also will be dangerous even if it occurs only for a short period.

Figures 21 and 22 demonstrate the variation of forces and moments versus the sideslip angle and the roll angle. The coefficients for lift, drag, and roll moment are practically constant; the coefficient for the yawing moment is insignificant. The coefficients for lateral force and roll moment increase linearly from zero upward with increasing sideslip angle and roll angle. For instance a sideslip of +8 degrees toward starboard causes a lateral force toward port of eight times the value brought about by –8 degrees rolling toward starboard; the roll moment due to a sideslip is 70 percent higher. Both roll moments relative to the keel point are stabilizing, i.e., any rolling will reduce itself and a sideslip will produce a rolling toward the inside of the curve.

Simultaneous systematic variations of the angles of attack, of rolling, and of sideslip produced only unessential differences relative to drag and lateral forces compared with the separate variations. But the situation deteriorated relative to the lift. For a sideslip angle around 10 degrees the flow separated throughout. Lift then broke down much more completely as the additional rolling increased (Fig. 23).

Summing up, it can be stated:

1. The range of the angle of attack of the profiles of a dihedral foil with a circle segment characteristic which can be utilized is about –4 degrees $< \alpha <$ +6 degrees.

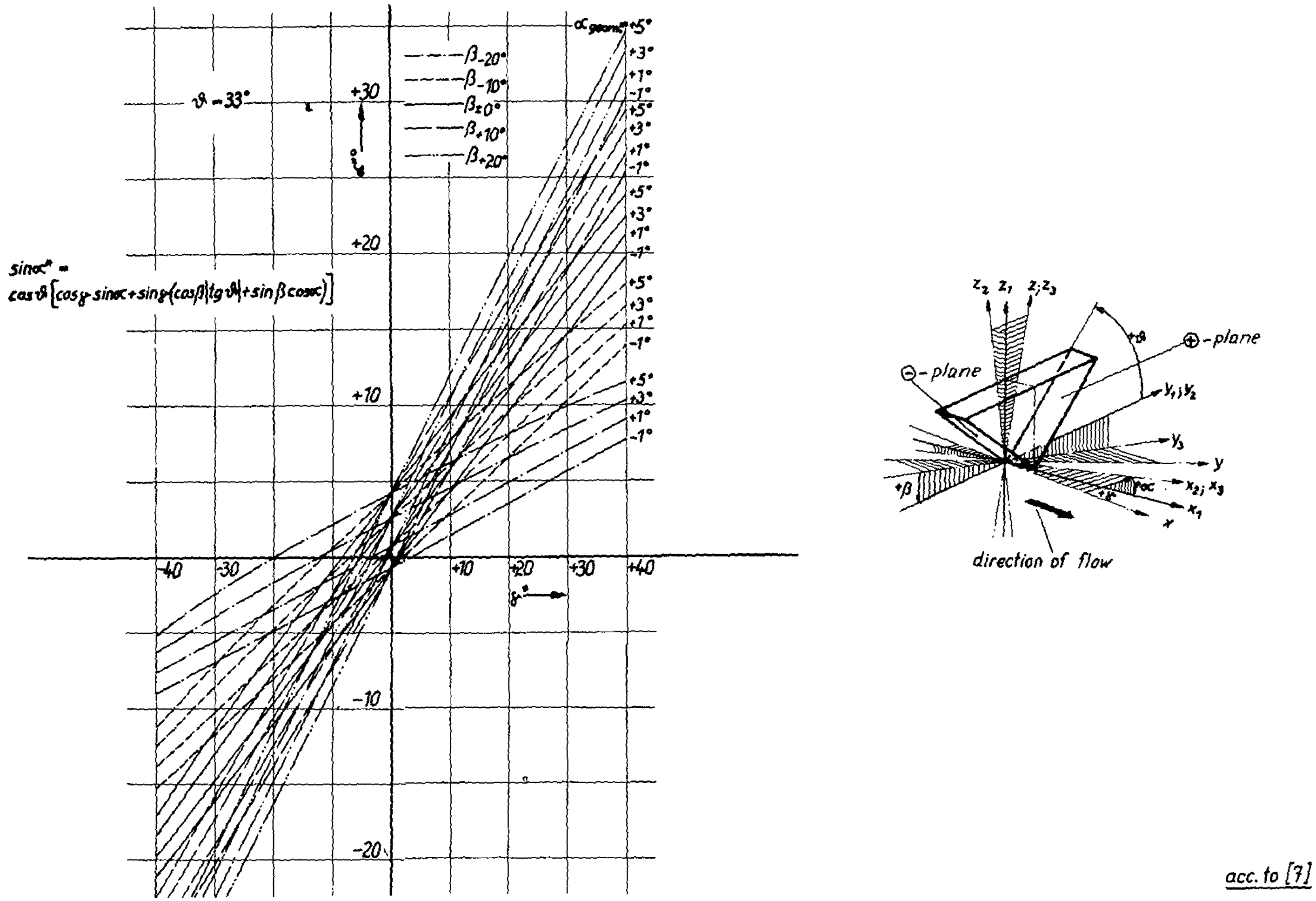

Fig. 18. Effective angle of attack of the chord

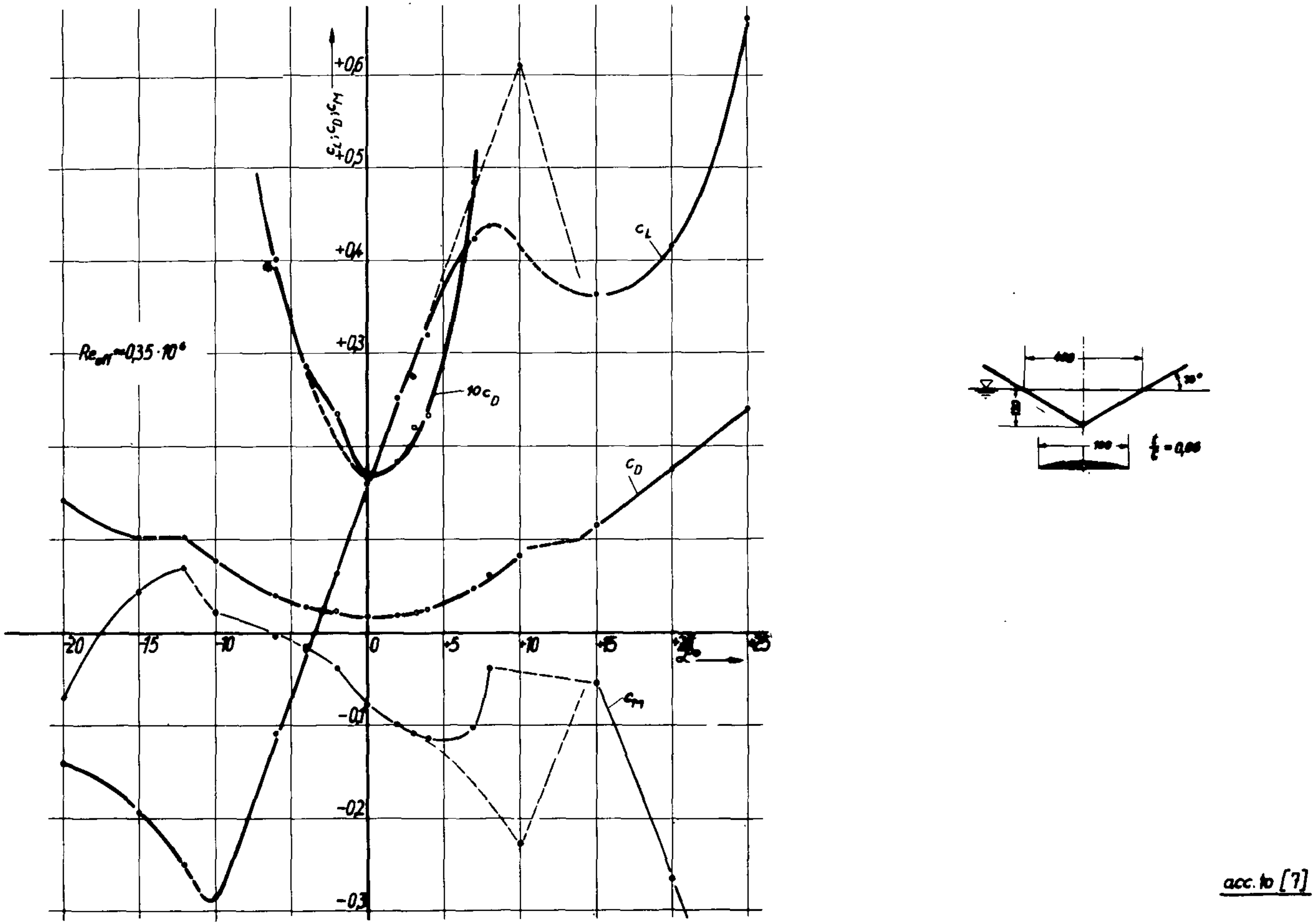

Fig. 19. Lift, drag, and pitching moment for a dihedral foil in a symmetrical flow

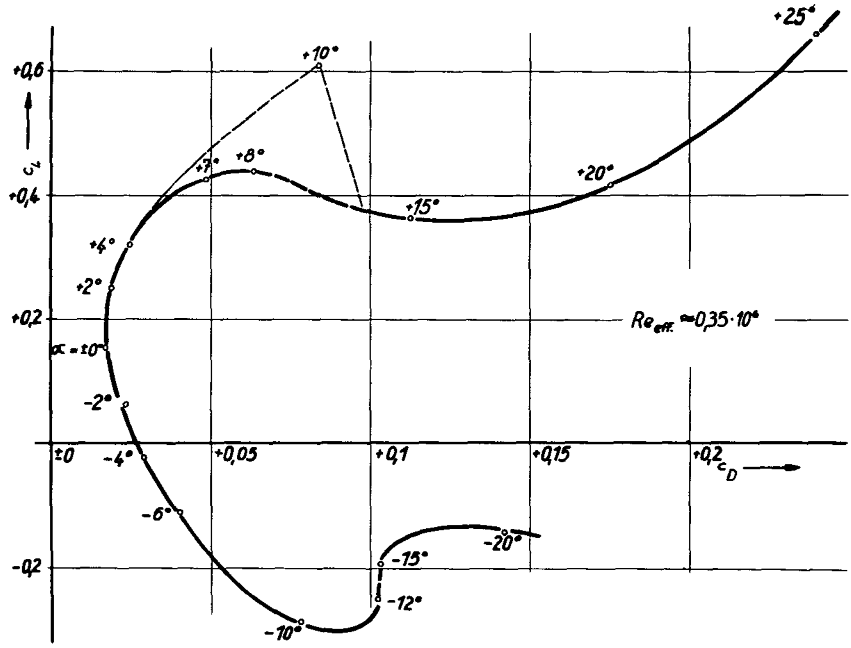

acc. to (7)

Fig. 20. Polar of a dihedral foil in a symmetrical flow

2. Lateral stabilizing can be brought about much more effectively by the moment due to sideslip than by that due to rolling. While the rolling is less dangerous for the lift, a range of only +8 degrees can be admitted for a sideslip angle.

3. Additional rolling of a dihedral foil in a sideslip motion acting in the same sense as the moment due to sideslip will raise the risk of a lift breakdown.

EXAMINATION OF ROTARY INSTABILITY

With a model of a dihedral foil the relation between rolling and sideslip has been tested thoroughly in a small VWS tank using a special device (Fig. 24). For a constant lift, the model at $u_o = 4$ m/sec could immerse freely. Relative to rotary motions both about the longitudinal and the vertical axis the model could either be fixed or set free.

The sideslip angle was measured each time when the lift collapsed. For free rolling, sideslip angles up to 11 degrees could be brought about; rolling angles then amounted to about 10 degrees acting in the same direction as the moment due to the sideslip. Enlarging the sideslip angle to 11 degrees caused a lift breakdown at the foil which had been more emerging and a rotary instability was the result. This procedure is not reversible, i.e., the sideslip angle has to be totally reduced to regain the flow and to start with sideslip again. For a fixed rolling of 20 degrees, sideslip angles of 16 degrees and 9 degrees could be obtained; the smaller sideslip angle is conjugated to rolling in the same sense as the moment due to sideslip, the other one is conjugated to rolling in the opposite direction.

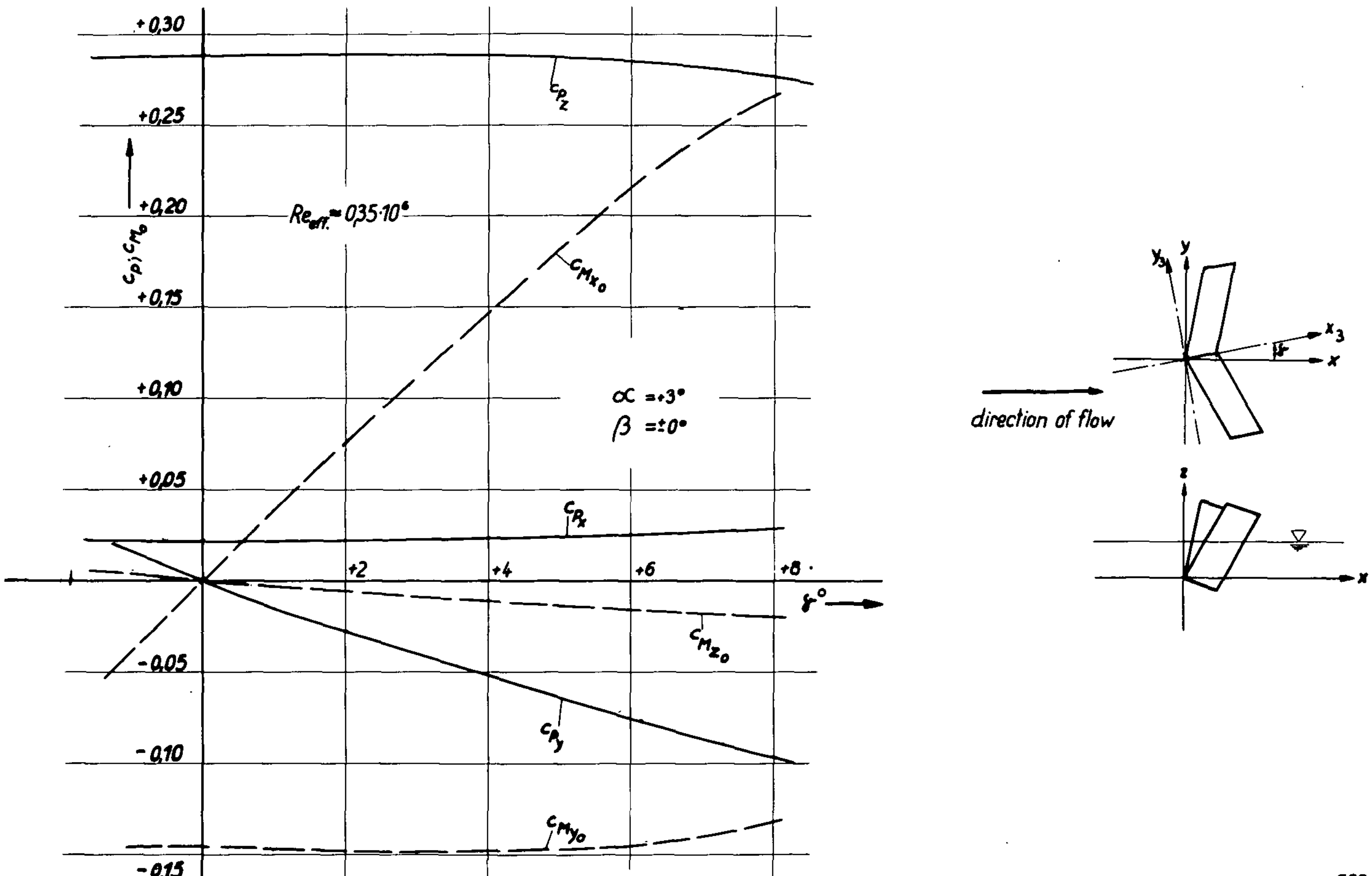

acc. to [7]

Fig. 21. Forces and moments for small sideslip angles.

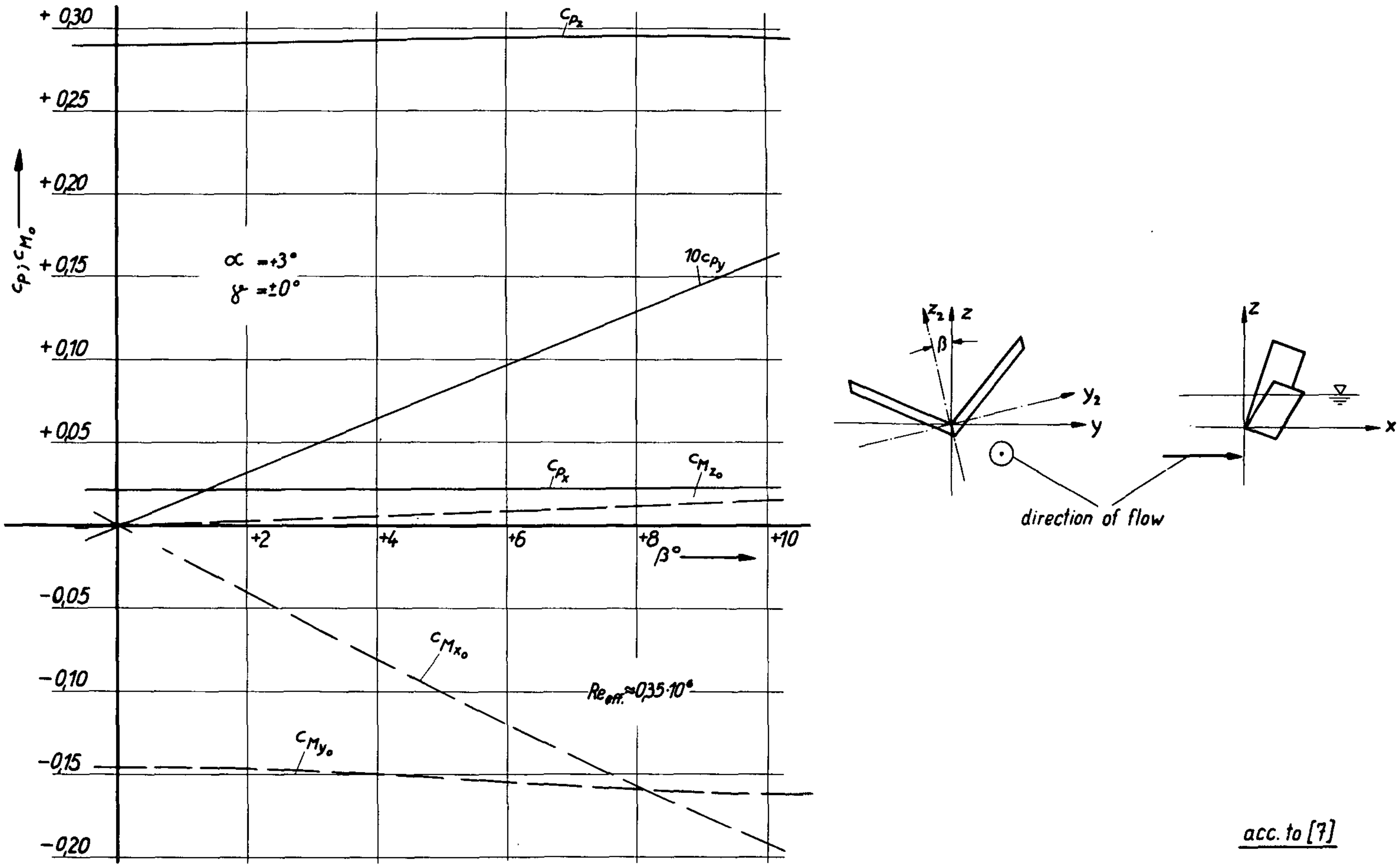

acc. to [7]

Fig. 22. Forces and moments for small roll angles

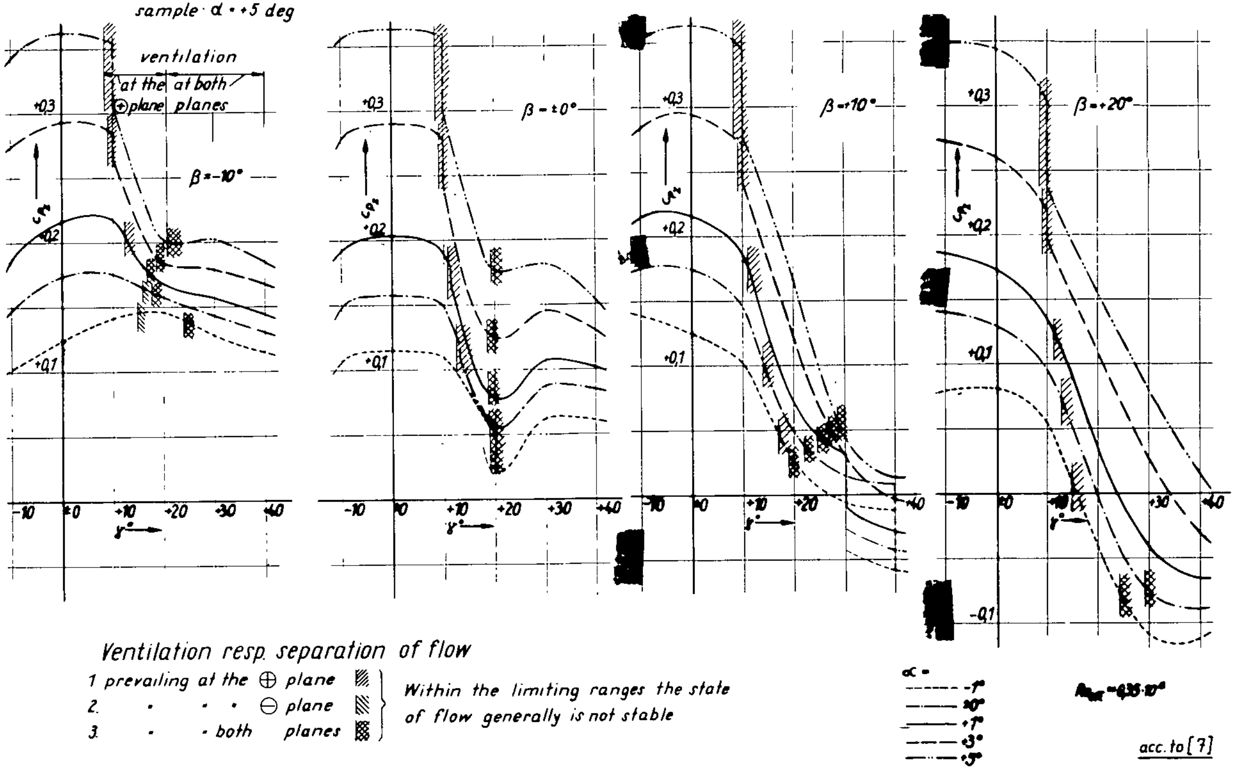

Fig. 23. Dimensionless lift C_{P_x}

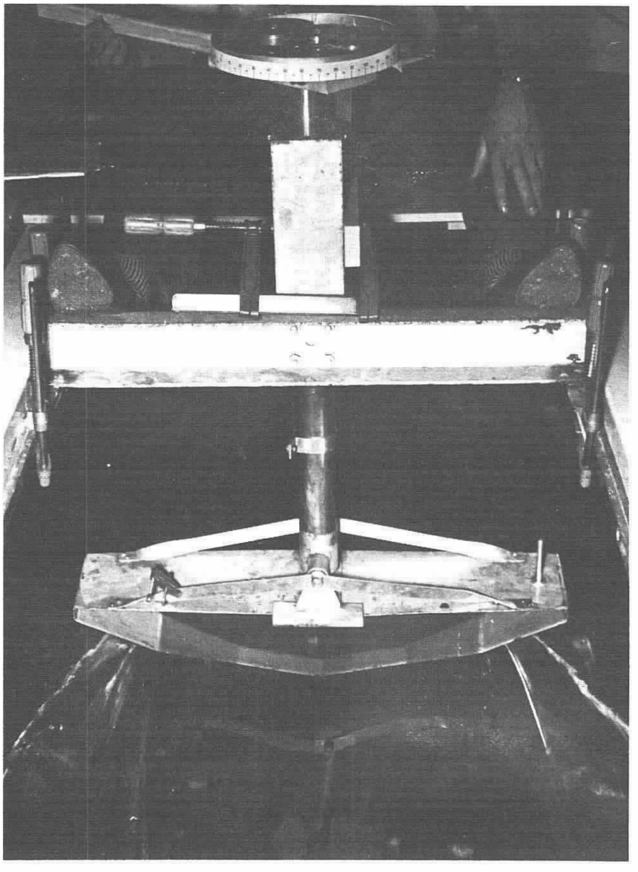

Fig. 24. Arrangement for rotary instability tests of a dihedral foil

To sum up:

1. Rolling into the inside of the curve for hydrofoil boats as well as for planing craft and airplanes such that the principal plane coincides with the apparent perpendicular is more disadvantageous relative to security than is rolling into the outside of the curve as occurs with displacement craft.

2. Hydrofoils already rolling to the outside at the beginning of the curve will run a tighter circle (with higher sideslip angles) than those rolling to the inside.

3. The preceding result contradicts the conception that in a circle a foil rolling to the outside will stall easier because of the higher load. Therefore the whole situation needs a thorough investigation.

THEORETICAL CONSIDERATIONS

The velocity field of a hydrofoil of great span running at the depth $\bar{h} = h/c = h^*/2$ beneath the undisturbed water surface in deep water can be represented by the well-known relations (for instance, Ref. 8)

$$\frac{u(x,z)}{u_0} = 1 + \frac{u_1(x,z)}{u_0}$$

$$= 1 + \frac{1}{2\pi}\int_{-1}^{+1} f(\xi)\,\frac{z + h^*}{(x-\xi)^2 + (z+h^*)^2}\,d\xi$$

$$+ \frac{1}{2\pi}\int_{-1}^{+1} f(\xi)\,\frac{z - h^*}{(x-\xi)^2 + (z-h^*)^2}\,d\xi \tag{1}$$

$$+ \frac{g}{u_0^2}\exp\left[-\frac{g}{u_0^2}(h^* - z)\right]\int_{-1}^{+1} f(\xi)\,G_1\left(\frac{g}{u_0^2}, x, \xi, z, h^*\right)d\xi \tag{1a}$$

$$\frac{w(x,z)}{u_0} = \frac{w_1(x,z)}{u_0}$$

$$= -\frac{1}{2\pi}\int_{-1}^{+1} f(\xi)\,\frac{x-\xi}{(x-\xi)^2 + (z+h^*)^2}\,d\xi$$

$$-\frac{1}{2\pi}\int_{-1}^{+1} f(\xi)\,\frac{x-\xi}{(x-\xi)^2 + (z-h^*)^2}\,d\xi$$

$$-\frac{g}{u_0^2}\exp\left(-\frac{g}{u_0^2}[h^* - z]\right)\int_{-1}^{+1} f(\xi)\,G_2\left(\frac{g}{u_0^2}, x, \xi, z, h^*\right)d\xi \tag{1b}$$

where u_o denotes the running speed and $f(\xi)$ the pressure distribution over the profile length. At the free surface the velocity field fulfils the boundary condition resulting from the linearized Bernoulli law

$$\frac{u_0^2}{g}\,\frac{\partial u_1(x,0)}{\partial x} + w_1(x,0) = 0. \tag{2}$$

The shape of the surface results as well from the Bernoulli law by linearization to

$$z_w(x) = -\frac{u_0 u_1(x,0)}{g} . \tag{3}$$

The pressure distribution at the profile, i.e., the function $f(\xi)$ with $f(x)$ being the meanline of the profile, can be found from the relation

$$u(x,-h^*)\ f'(x) = w(x,-h^*) \tag{4}$$

with u and w taken from Eq. (1).

The boundary condition (2) and hence the velocity field (1) is valid for smooth water above the foil as well as ahead and aft, i.e., for a condition which permits the existence of deep water waves.

Within the technically interesting range of the Froude depth number $F_h = u_o\sqrt{gh}$ there is as shown by experimental investigations rapid flow prevailing above the foil with the exception of the direct neighborhood of the leading edge. For this case the boundary condition (2) and therewith the terms for the velocity field (1) are no longer valid. Behind the foil, with the exception of the direct neighborhood of the trailing edge, the flow is tranquil again, for here the physical suppositions for rapid flow are missing due to the water presumed as being deep. For this range Eqs. (1) and (2) are valid again.

The consequence of the rapid flow is that the water surface above the foil remains smooth, while for small distances between foil and water surface the water flows parallel to the upper side of the profile, whereby the well-known apparent camber reduction results. That means above the foil there is, dependent on the Froude depth number, at relative low speeds already a state of flow which will occur behind the foil only at considerably higher speeds. Therefore for the range of the foil ($-1 > x > +1$) in Eqs. (1) the terms containing $g/u_o{}^2$ may equal 0. The equations simplify to

$$\begin{aligned}\frac{u(x,z)}{u_0} = 1 &+ \frac{1}{2\pi}\int_{-1}^{+1} f(\xi)\ \frac{(z+h^*)\ d\xi}{(x-\xi)^2 + (z+h^*)^2} \\ &+ \frac{1}{2\pi}\int_{-1}^{+1} f(\xi)\ \frac{(z-h^*)\ d\xi}{(x-\xi)^2 + (z-h^*)^2}\end{aligned} \tag{5a}$$

$$\begin{aligned}\frac{w(x,z)}{u_0} = &-\frac{1}{2\pi}\int_{-1}^{+1} f(\xi)\ \frac{(x-\xi)\ d\xi}{(x-\xi)^2 + (z+h^*)^2} \\ &-\frac{1}{2\pi}\int_{-1}^{+1} f(\xi)\ \frac{(x-\xi)\ d\xi}{(x-\xi)^2 + (z-h^*)^2} .\end{aligned} \tag{5b}$$

At the surface ($z = 0$) the additional velocity u_1 in Eqs. (5) disappears, so that in the case of rapid flow at the upper side of the profile the boundary condition

$$\frac{u(x,0)}{u_0} = 1 \tag{6}$$

will be satisfied.

By inserting the velocity components (5) into (4) the following integral equation for determining the pressure distribution $f(\xi)$ results:

$$-2\pi f'(x) = \int_{-1}^{+1} f(\xi) \left[\frac{1}{x - \xi} + \frac{(x-\xi) - 2h^* f'(x)}{(x-\xi)^2 + 4h^{*2}} \right] d\xi \,. \tag{7}$$

The integral

$$\int_{-1}^{+1} f(\xi) \frac{d\xi}{x - \xi}$$

is the known relation for the downwash of a thin profile in an infinite medium. The part of the relation (7) dependent on the depth of submergence h^* represents the influence of the surface, which results in a diminution of the effective angle of incidence for the profile.

For the solution of Eq. (7) the following function with unknown coefficients will be chosen:

$$f(\xi) = 2a_0 \sqrt{\frac{1-\xi}{1+\xi}} + 4a_1 \sqrt{1-\xi^2} + 4a_2 \xi \sqrt{1-\xi^2} \,. \tag{8}$$

The coefficients a_n will be found by complying with Eq. (7) for three points of the chord. For these points $x = \pm c/4$ and $x = \pm 0$ may be chosen. By means of the a_n, which are a function of h^*, the lift of the profile follows from the known relation

$$C_L \equiv C_L(h^*) = 2\pi \left[a_0(h^*) + a_1(h^*) \right] . \tag{9}$$

If the distance h^* is considerable, i.e., if the profile is deeply submerged, it then follows from (7) that

$$-2\pi f'(x) = \int_{-1}^{+1} f(\xi) \frac{d\xi}{x - \xi} \,, \tag{7a}$$

that is, the Ackermann-Birnbaum integral equation for evaluating the pressure distribution of thin profiles in infinite flow. If the distance h^* disappears, i.e., if the profile runs at the surface, it then follows from (7) that

$$-\pi f'(x) = \int_{-1}^{+1} f(\xi) \frac{d\xi}{x - \xi} \,. \tag{7b}$$

646551 O—62——13

The lift then has only one-half the magnitude it has in great depth; that means in this case only the lift of the lower side is effective.

Now a curved profile may be considered, for instance a circle segment profile with camber m and angle of incidence α_{geom} of the chord. For this the contour of the chord is given by

$$f(x) = f_0 x + f_1 x^2 . \tag{10}$$

Then

$$f'(x) = f_0 + 2f_1 x \tag{11}$$

where f_0 and f_1 may be of small values:

$$f_0 = -\alpha_{geom}$$

$$f_1 = -2m .$$

For this case Eq. (1) can be written

$$-2\pi' f_0 = \int_{-1}^{+1} f(\xi) \left[\frac{1}{x-\xi} + \frac{(x-\xi) - 2h^* f_0}{(x-\xi)^2 + 4h^{*2}} \right] d\xi \tag{12a}$$

$$-4\pi' f_1 x = \int_{-1}^{+1} f(\xi) \left[\frac{1}{x-\xi} + \frac{(x-\xi) - 4h^* f_1 x}{(x-\xi)^2 + 4h^{*2}} \right] d\xi . \tag{12b}$$

Equation (12a) gives the lift of a flat plate,

$$C_{L_0}(h^*) = 2\pi \left[a_{00}(h^*) + a_{10}(h^*) \right]$$

and Eq. (12b) gives the additional lift produced by the camber,

$$C_{L_1}(h^*) = 2\pi \left[a_{01}(h^*) + a_{11}(h^*) \right] .$$

The total lift then amounts to

$$C_L(h^*) = C_{L_0}(h^*) + C_{L_1}(h^*)$$

and is shown in Fig. 25 for a flat plate as well as for a circle segment profile.

For the profile approaching the surface an apparent camber reduction at the upper side occurs whereby the lift of the profile, already reduced by the proximity of the surface, will be reduced further. In the actual case of a circle segment profile the lower side is flat; it is therefore equal to the lower side of a flat plate and delivers a lift taken as independent of the depth h^*:

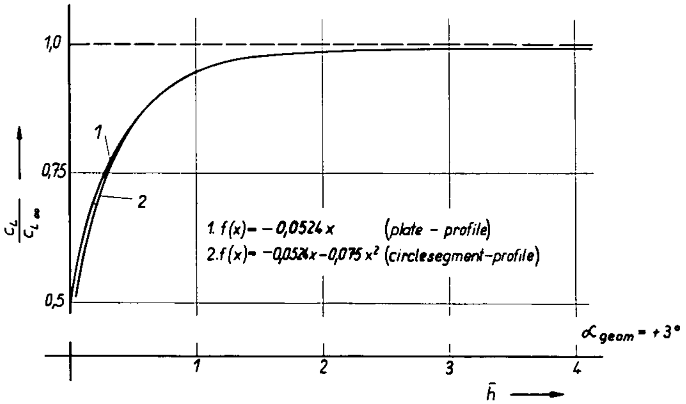

Fig. 25. Decrease of lift near the surface without regard to the apparent camber reduction

$$C_L(h^*)\Big|_{\ell s} = C_{L_0}(\infty)\Big|_{\ell s} = 2\pi\,\frac{a_{00}(\infty)}{2}\,, \tag{13}$$

$$\frac{C_L(h^*)}{C_L(\infty)}\Bigg|_{\ell s} = 1\,.$$

The lift of the upper side can be written

$$\begin{aligned} C_L(h^*)\Big|_{us} &= C_{L_0}(h^*)\Big|_{us} + C_{L_1}(h^*)\Big|_{us} \\ &= 2\pi\left\{a_{00}(h^*) - \frac{a_{00}(\infty)}{2} + a_{10}(h^*)\right. \\ &\qquad \left. + \sigma\left(\frac{h^*}{2}\right)\left[a_{01}(h^*) + a_{11}(h^*)\right]\right\}\,, \end{aligned} \tag{14}$$

$$\begin{aligned} \frac{C_L(h^*)}{C_L(\infty)}\Bigg|_{us} = \frac{1}{0{,}5\;a_{00}(\infty) + a_{11}(\infty)} &\left\{a_{00}(h^*) - \frac{a_{00}(\infty)}{2} + a_{10}(h^*)\right. \\ &\left. + \sigma\left(\frac{h^*}{2}\right)\left[a_{01}(h^*) + a_{11}(h^*)\right]\right\} \end{aligned}$$

where $\sigma(h^*/2)$ stands the apparent camber reduction. The total lift of the profile then amounts to

$$C_L(h^*) = C_L(h^*)\Big|_{us} + C_L(h^*)\Big|_{\ell s}$$

$$= 2\pi\left\{a_{00}(h^*) + a_{10}(h^*) + \sigma\left(\frac{h^*}{2}\right)\left[a_{01}(h^*) + a_{11}(h^*)\right]\right\} , \qquad (15)$$

$$\frac{C_L(h^*)}{C_L(\infty)} = \frac{a_{00}(h^*) + a_{10}(h^*) + \sigma\left(\frac{h^*}{2}\right)\left[a_{01}(h^*) + a_{11}(h^*)\right]}{a_{00}(\infty) + a_{11}(\infty)}$$

where

$$a_{00}(\infty) = \alpha = -f_0$$

$$a_{11}(\infty) = 2m = -f_1 .$$

In Eq. (15) only the factor $\sigma(h^*/2)$ is unknown. It can be calculated theoretically, but then separate mathematical operations will be necessary. By experiment this camber reduction factor can be found easily from the reduction of the no-lift angle occurring in an approach to the surface

$$\sigma\ \frac{h^*}{2} \equiv \sigma(\bar{h}) = \frac{\alpha_0(\bar{h})}{\alpha_0(\infty)} = \frac{m(\bar{h})}{m(\infty)} , \qquad (16)$$

where independence of the shape of the profile can be supposed. Figure (26) shows the factor $\sigma(\bar{h})$ as found by experiments. With the aid of this factor the lift reduction of the profile can be found as a function of the depth $\bar{h}$ from Eq. (15) as shown in Fig. 27.

Figure (28) shows the calculated lift of the upper side and of the lower side of the considered profile dependent on the depth $\bar{h}$, as well as the corresponding values taken by measurement. The actual increase of lift of the lower side and the decrease of lift of the upper

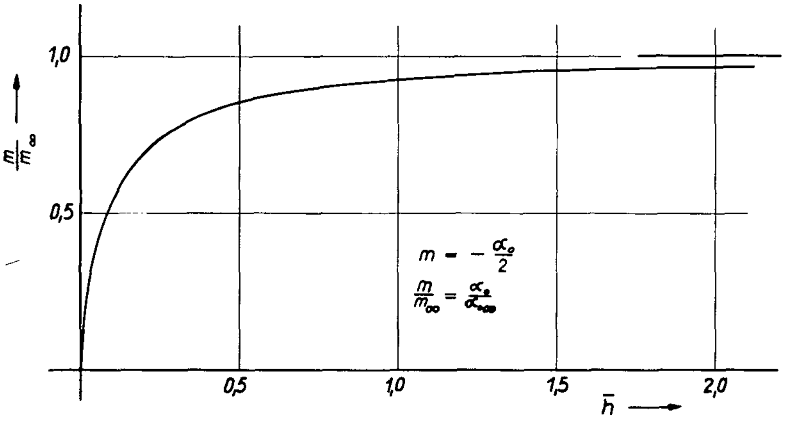

Fig. 26. Apparent camber reduction of a circle segment profile
as found experimentally

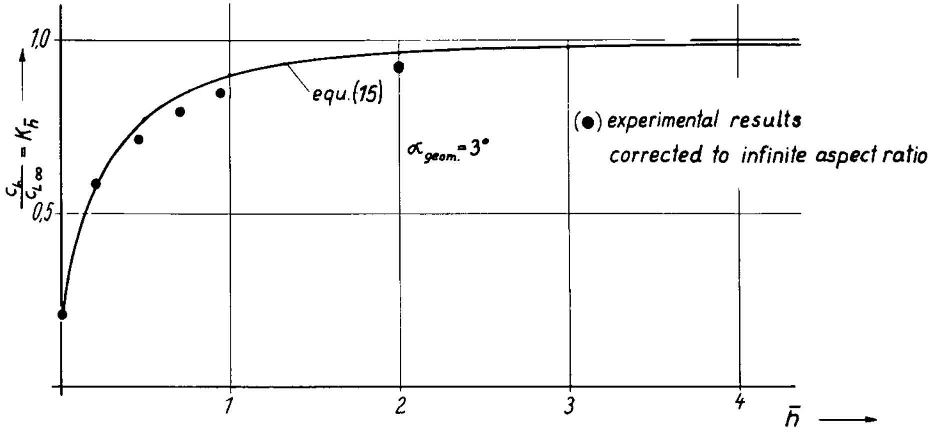

Fig. 27. Decrease of lift for a circle segment profile near the free surface

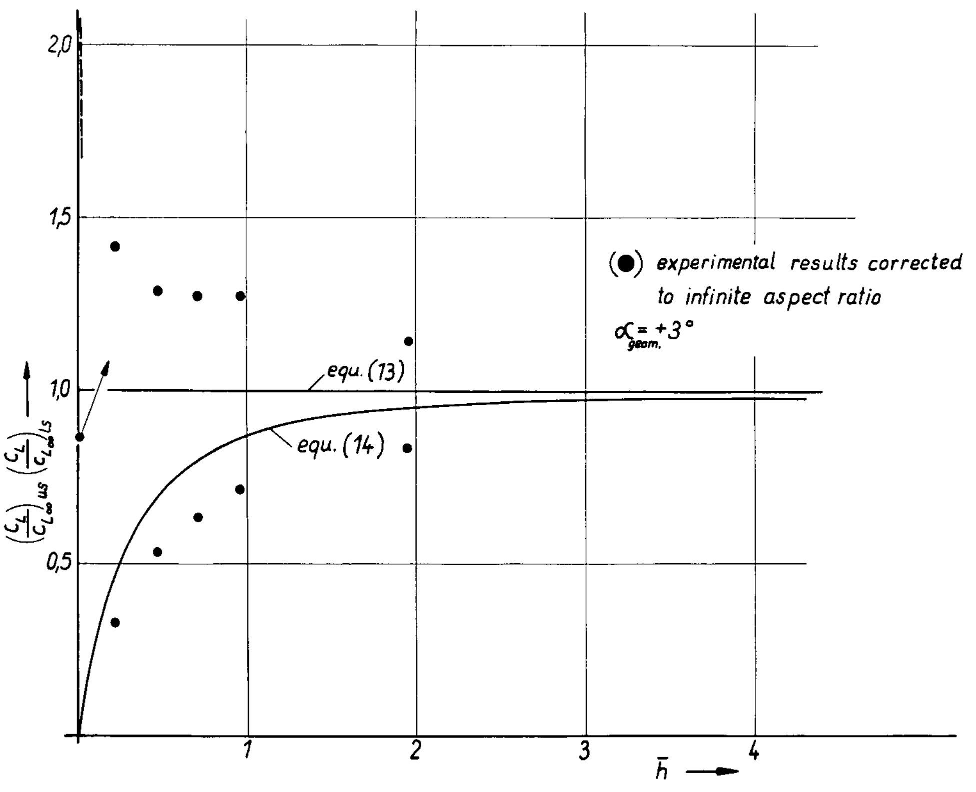

Fig. 28. Lift coefficients of the upper and lower sides of a circle segment profile.

side, being higher than calculated, cannot be represented by these simple formulas. But since these influences compensate each other for the most part, the calculated total lift nearly equals the measured lift. For calculating the total lift, therefore, this method may be used as an approximation.

INTRODUCTION OF THE MAIN PARAMETERS

Laying out foils for hydrofoil boats needs not only information about the decrease of lift due to the free surface but also about the influence of the aspect ratio and eventually of the dihedral angle. The above-mentioned measurements proved that for supercritical flow above the foils the spanwise distribution of lift is only slightly dependent on the depth $\bar{h}$. For supercritical flow, therefore, it is possible to consider the influences of the surface and of the aspect ratio separately without being greatly mistaken. Moreover this gives the possibility of calculating the lift decrease of dihedral foils.

The main parameters will be introduced now. The influence of the finite aspect ratio will be covered by the relation found by Weinig [9] by means of the cascade theory:

$$\frac{dC_L}{d\alpha} = K_A \; 2\pi \; . \tag{17}$$

The factor K_A is shown in Fig. 29. The aspect ratio of a dihedral foil has to be taken as the wetted aspect ratio, i.e.,

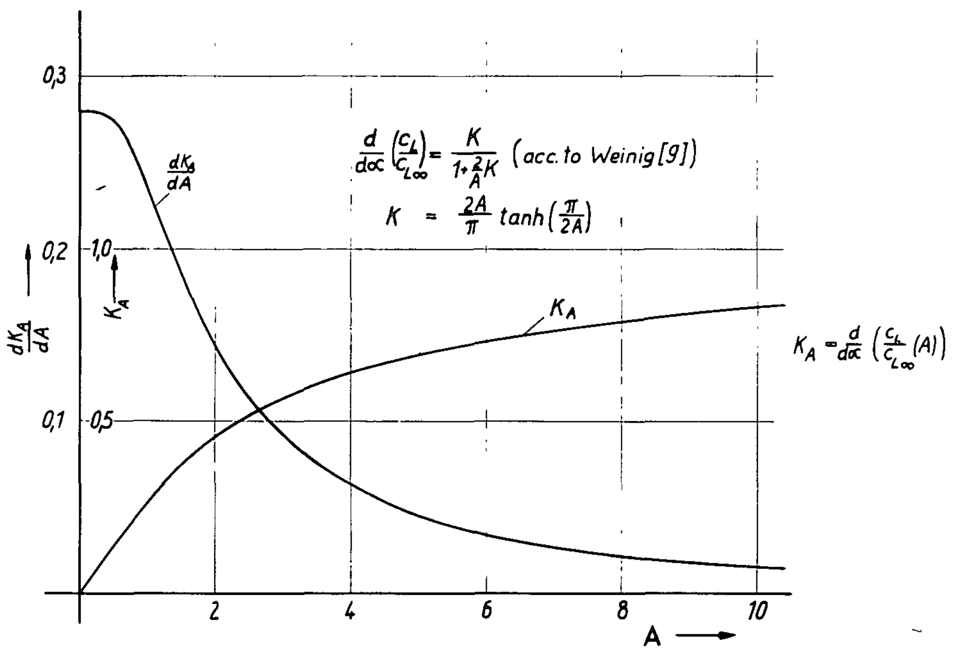

Fig. 29. Dependence of the lift gradient and the increase of the lift gradient on the aspect ratio

$$A = \frac{A_{\mathrm{proj}}}{\cos\vartheta}\,.$$

The parameter for the influence of the water surface $K_{\bar{h}}$ for parallel submerged foils equals the term

$$\frac{C_L}{C_{L\infty}}\,(\bar{h})$$

as shown in Fig. 30. For dihedral foils or slanting flat foils of constant profile length, the tips of which run at the depths $\bar{h}_1$ and $\bar{h}_2$ $(\bar{h}_2 > \bar{h}_1)$, a mean value valid for the whole foil can be found by integration of the term

$$\frac{C_L}{C_{L\infty}}\,(\bar{h})$$

over the depth of submergence:

$$K_{\bar{h}_m} = \frac{1}{\bar{h}_2 - \bar{h}_1}\int_{\bar{h}_1}^{\bar{h}_2}\frac{C_L}{C_{L\infty}}\,(\bar{h})d\bar{h}. \tag{18}$$

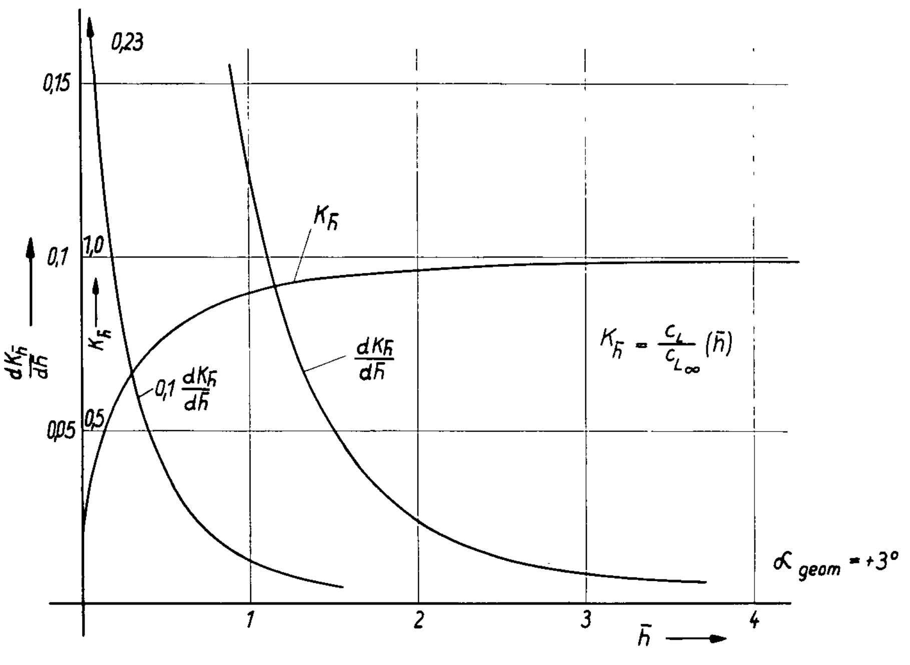

Fig. 30. Dependence of the decrease of lift and the gradient of the lift decrease on the depth ratio

In case the foil pierces the surface, $\bar{h}_1 = 0$ and the term shown in Fig. 31 is found to be

$$K_{\bar{h}_m} = \frac{1}{\bar{h}_2} \int_0^{\bar{h}_2} \frac{C_L}{C_{L\infty}} (\bar{h})\, d\bar{h} \,. \tag{18'}$$

One more parameter takes care of the difference between the geometrical angle of incidence α_{geom} generally defined for a system moving with the foils and the geometrical angle of incidence α^*_{geom} actually existing in a system fixed relative to flow. It may be stated (see Fig. 18)

$$K_\alpha = \frac{\alpha^*_{geom}}{\alpha_{geom}} = \frac{\cos\vartheta}{\sin\alpha_{geom}} \Big[\cos\gamma \sin\alpha_{geom} + \sin\gamma(\cos\beta|\tan\vartheta| + \sin\beta\cos\alpha_{geom})\Big] \,. \tag{19}$$

For a nonrolling and nonsideslipping dihedral foil with the dihedral angle ϑ,

$$K_\alpha = \cos\vartheta \,.$$

Together with the known profile efficiency factor K_P the increase of lift for a hydrofoil becomes

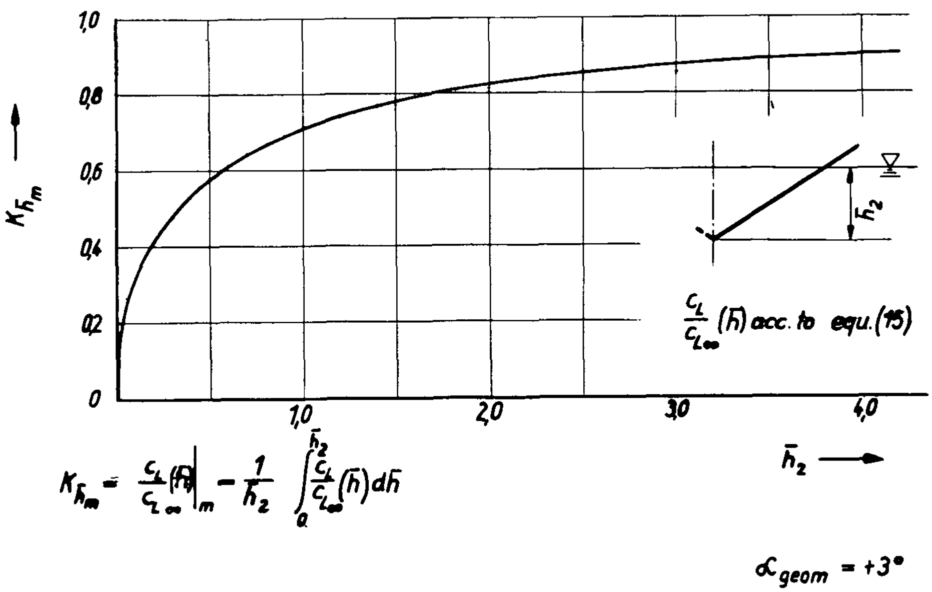

Fig. 31. Decrease of lift for a dihedral foil

$$\frac{dC_L}{d\alpha} = 2\pi\ K_A\ K_{\bar{h}}\ K_\alpha\ K_P\ . \tag{20}$$

By means of this relation the results of wind-tunnel tests or of theoretical calculations can be compared with the results of hydrofoil measurements.

VERTICAL STABILITY OF HYDROFOILS

For the sake of good driving properties a suitable vertical stability of hydrofoils is very important. However, it should again not be too great since the foils then will respond to minor disturbances, for instance to small waves on a surface otherwise calm; that means such foils will run stiff. Therefore not too steep a dL/dh curve is desirable.

For a nonrolling surface-piercing foil, the lowest point of which is at depth $\bar{h}_2$ with wetted aspect ratio A, the total change of lift

$$dL\Big|_{A,\bar{b},\bar{h}_2} = \frac{\partial L}{\partial A}\Big|_A\ dA + \frac{\partial L}{\partial \bar{b}}\Big|_{\bar{b}}\ d\bar{b} + \frac{\partial L}{\partial \bar{h}}\Big|_{0,\bar{h}_2}\ d\bar{h} \tag{21}$$

is dependent on the variations of aspect ratio, span, and depth of submergence. From the geometry of the foil it follows that

$$dA = \frac{d\bar{h}}{\sin\vartheta} = d\bar{b}$$

so that

$$\frac{dL}{d\bar{h}}\Big|_{A,\bar{b},\bar{h}_2} = \frac{\partial L}{\partial A}\Big|_A\ \frac{1}{\sin\vartheta} + \frac{\partial L}{\partial \bar{b}}\Big|_{\bar{b}}\ \frac{1}{\sin\vartheta} + \frac{\partial L}{\partial \bar{h}}\Big|_{0,\bar{h}_2}\ .$$

From

$$L = \rho u_0^2\, bc\, C_{L\infty} K_\alpha\ K_P\ \cos\vartheta\ K_A\ K_{\bar{h}_m} \tag{22}$$

it follows that for each panel of the foil

$$\frac{\partial L}{\partial A}\Big|_A = \frac{1}{2}\rho u_0^2\, b\, c\, C_{L\infty} K_\alpha K_P\ \cos\vartheta\ \frac{\partial K_A}{\partial A}\Big|_A\ K_{\bar{h}_m}\Big|_{\bar{h}_2} \tag{23a}$$

$$\frac{\partial L}{\partial \bar{b}}\Big|_{\bar{b}} = \frac{1}{2}\rho u_0^2\, b\, c\, C_{L\infty} K_\alpha K_P\ \cos\vartheta\ \frac{1}{\bar{b}}\ K_A\Big|_A\ K_{\bar{h}_m}\Big|_{\bar{h}_2} \tag{23b}$$

$$\frac{\partial L}{\partial \bar{h}}\Big|_{0,\bar{h}_2} = \frac{1}{2}\rho u_0^2\, b\, c\, C_{L\infty} K_\alpha K_P\ \cos\vartheta\ K_A\Big|_A\ \frac{\partial K_{\bar{h}_m}}{\partial \bar{h}}\Big|_{0,\bar{h}_2}\ . \tag{23c}$$

The quantity $\partial K_A/\partial A$ may be taken from Fig. 29. Furthermore

$$\frac{\partial K_{\bar{h}_m}}{\partial \bar{h}} = \frac{\partial}{\partial \bar{h}}\left(\frac{1}{\bar{h}_2}\int_0^{\bar{h}_2} K_{\bar{h}}\, d_{\bar{h}}\right) = \frac{1}{\bar{h}_2}\left(K_{\bar{h}}\Big|_{\bar{h}_2} - K_{\bar{h}_m}\Big|_{\bar{h}_2}\right)$$

with $K_{\bar{h}}$ and $K_{\bar{h}_m}$ being as given by Figs. 30 and 31. Herewith the heaving gradient becomes

$$\left.\frac{dL}{d\bar{h}}\right|_{A_1\bar{b}_1\bar{h}_2} = \rho u_0^2\, b\, c\, C_{L\infty} K_\alpha K_P \cos\vartheta \left[\left.\frac{\partial K_A}{\partial A}\right|_A \frac{K_{\bar{h}_m}\Big|_{\bar{h}_2}}{\sin\vartheta} + K_A\Big|_A \frac{K_{\bar{h}_m}\Big|_{\bar{h}_2}}{\bar{b}\sin\vartheta} + K_A\Big|_A \frac{1}{\bar{h}_2}\left(K_{\bar{h}}\Big|_{\bar{h}_2} - K_{\bar{h}_m}\Big|_{\bar{h}_2}\right)\right] \tag{24a}$$

and

$$\left.\frac{dC_L}{d\bar{h}}\right|_{A_1\bar{b}_1\bar{h}_2} = C_{L\infty} K_\alpha K_P \cos\vartheta \left\{\left.\frac{\partial K_A}{\partial A}\right|_A \frac{K_{\bar{h}_m}\Big|_{\bar{h}_2}}{\sin\vartheta} + K_A\Big|_A \left(\frac{K_{\bar{h}_m}\Big|_{\bar{h}_2}}{\bar{b}\sin\theta} + \left.\frac{K_{\bar{h}} - K_{\bar{h}_m}}{\bar{h}}\right|_{\bar{h}_2}\right)\right\} \tag{24b}$$

with $C_{L\infty} = 2\pi \sin(\alpha + 2m)$.

In the case of a submerged dihedral foil or a flat parallel submerged foil the change of lift due to changes of submergence will be remarkably less than for the surface-piercing dihedral foil, because the first two terms of Eq. (24b) disappear. For a flat foil running at depth $\bar{h}_0$ the depth-gradient becomes

$$\left.\frac{dL}{d\bar{h}}\right|_{A_1\bar{b}_1\bar{h}_0} = \rho u_0^2\, b\, c\, C_{L\infty} K_P K_A\Big|_A \left.\frac{\partial K_{\bar{h}}}{\partial \bar{h}}\right|_{\bar{h}_0} \qquad (K_\alpha = 1) \tag{25a}$$

and

$$\left.\frac{dC_L}{d\bar{h}}\right|_{A_1\bar{b}_1\bar{h}_0} = C_{L\infty} K_P K_A\Big|_A \left.\frac{\partial K_{\bar{h}}}{\partial \bar{h}}\right|_{\bar{h}_0} . \tag{25b}$$

It can be seen here that for the range of a small depth of submergence ($\bar{h}_0 \leq 1$) a vertical stabilization of a flat foil is quite possible as confirmed by experiments made in the Berlin Towing Tank with such a foil in a seaway. The submerged dihedral foil proved to be much more unfavorable since only those parts running near the surface are strongly influenced by the surface effect. In this case with the lowest point of the foil at depth $\bar{h}_2$ and the highest point at depth $\bar{h}_1$,

$$\left.\frac{dL}{d\bar{h}}\right|_{A_1\bar{b}_1\bar{h}_1,\bar{h}_2} = \rho u_0^2\, b\, c\, C_{L\infty} K_\alpha K_P \cos\vartheta \left. K_A\right|_A \left.\frac{\partial K_{\bar{h}_m}}{\partial \bar{h}}\right|_{\bar{h}_1,\bar{h}_2} . \tag{26a}$$

Thus

$$\left.\frac{\partial K_{\bar{h}_m}}{\partial \bar{h}}\right|_{\bar{h}_1,\bar{h}_2} = \frac{\partial}{\partial \bar{h}}\left(\frac{1}{\bar{h}_1 - \bar{h}_2}\int_{\bar{h}_1}^{\bar{h}_2} K_{\bar{h}}\, d\bar{h}\right) = \frac{1}{\bar{b}\sin\vartheta}\left(\left.K_{\bar{h}}\right|_{\bar{h}_2} - \left.K_{\bar{h}}\right|_{\bar{h}_1}\right).$$

This gives

$$\left.\frac{dC_L}{d\bar{h}}\right|_{A_1\bar{b}_1\bar{h}_1,\bar{h}_2} = C_{L\infty} K_\alpha K_P \cos\vartheta \left. K_A\right|_A \frac{\left.K_{\bar{h}}\right|_{\bar{h}_2} - \left.K_{\bar{h}}\right|_{\bar{h}_1}}{\bar{b}\sin\vartheta} . \tag{26b}$$

An improvement for the submerged dihedral foil will be possible by arranging horizontal auxiliary foils at the upper ends as near as possible to the surface such that they are within the range of substantial $\partial K_{\bar{h}}/\partial \bar{h}$ (Fig. 30).

ROLLING STABILITY

A surface-piercing nonrolling dihedral foil with the dihedral angle ϑ, constant profile length, and wetted aspect ratio A may be examined now. For an inclination $d\beta$ a differential stabilizing moment relative to the lowest point is produced according to

$$\left. dM_x\right|_{A_1\bar{b}_1\bar{h}_2} = \left.\frac{\partial M_x}{\partial A}\right|_A dA + \left.\frac{\partial M_x}{\partial \bar{b}}\right|_{\bar{b}} d\bar{b} + \left.\frac{\partial M_x}{\partial \bar{h}}\right|_{0,\bar{h}_2} d\bar{h} . \tag{27}$$

The differentials dA, $d\bar{b}$, and $d\bar{h}$ can be obtained from the geometry of the foil:

$$d\bar{b} = \mp\, d\beta \frac{1}{\tan\vartheta} = dA$$

$$d\bar{h} = \mp\, d\beta\, \bar{b}\, \bar{\eta} \cos\vartheta$$

with the dimensionless distance from the lowest point $\bar{\eta} = \eta/b$. For evaluating $\partial M_x/\partial A$, $\partial M_x/\partial \bar{b}$, and $\partial M_x/\partial \bar{h}$ the spanwise lift distribution will be given by the term $f(\bar{\eta},\bar{h}) = f(\bar{\eta})\, f(\bar{h})$, where with sufficient accuracy an elliptical law may be chosen for the function $f(\bar{\eta})$:

$$f(\bar{\eta}) = C_L(\bar{\eta}) = C_{L\infty} K_A \frac{4}{\pi}\sqrt{1 - \bar{\eta}^2} .$$

The function $f(\bar{\eta})$ takes care of the depth of submergence, i.e.,

$$f(\bar{h}) = \frac{C_L}{C_{L\infty}} = K_{\bar{h}}$$

where

$$\begin{aligned}\bar{h} &= \bar{h}_2(1 - \bar{\eta}) \\ &= \bar{h}_2 - \bar{b}\,\bar{\eta}\sin\vartheta\,.\end{aligned}$$

Herewith the moment M_x may be written as

$$M_x = \rho u_0^2\, b\, c^2 C_{L\infty} K_\alpha K_P \bar{b} K_A \frac{4}{\pi} \int_0^1 \bar{\eta}\sqrt{1 - \bar{\eta}^2}\, K_{\bar{h}}\Big|_{\bar{\eta}}\, d\bar{\eta}\,. \tag{28}$$

The derivatives of the moments relative to the single parameters are

$$\left.\frac{\partial M_x}{\partial A}\right|_{A_1\bar{b}_1\bar{h}_2} = \frac{1}{2}\rho u_0^2\, b\, c^2 C_{L\infty} K_\alpha K_P \bar{b} \left.\frac{\partial K_A}{\partial A}\right|_A \frac{4}{\pi}\int_0^1 \bar{\eta}\sqrt{1-\bar{\eta}^2}\, K_{\bar{h}}\Big|_{\bar{\eta}}\, d\bar{\eta} \tag{29a}$$

$$\left.\frac{\partial M_x}{\partial \bar{b}}\right|_{A_1\bar{b}_1\bar{h}_2} = \frac{1}{2}\rho u_0^2\, b\, c^2 C_{L\infty} K_\alpha K_P K_A\Big|_A \frac{8}{\pi}\int_0^1 \bar{\eta}\sqrt{1-\bar{\eta}^2}\, K_{\bar{h}}\Big|_{\bar{\eta}}\, d\bar{\eta} \tag{29b}$$

$$\left.\frac{\partial M_x}{\partial \bar{h}}\right|_{A_1\bar{b}_1\bar{h}_2} = \frac{1}{2}\rho u_0^2\, b\, c^2 C_{L\infty} K_\alpha K_P \bar{b}\, K_A\Big|_A \frac{4}{\pi}\int_0^1 \bar{\eta}\sqrt{1-\bar{\eta}^2}\, \left.\frac{\partial K_{\bar{h}}}{\partial \bar{h}}\right|_{\bar{\eta}} d\bar{\eta}\,. \tag{29c}$$

Herewith the total change of moment relative to the lowest point of the dihedral becomes

$$\frac{\partial M_x}{d\beta}_{A_1\bar{b}_1\bar{h}_2} = -\rho u_0^2\, b\, c^2 C_{L\infty} K_\alpha K_P \cos\vartheta\; \bar{b}^2 \frac{4}{\pi}\left[\left.\frac{\partial K_A}{\partial A}\right|_A \frac{F_1}{\sin\vartheta} + K_A\Big|_A\left(\frac{2F_1}{\bar{b}\sin\vartheta} + F_2\right)\right] \tag{30a}$$

and

$$\left.\frac{dC_{M_x}}{d\beta}\right|_{A_1\bar{b}_1\bar{h}_2} = -C_{L\infty} K_\alpha K_P \cos\vartheta\; \bar{b}^2 \frac{4}{\pi}\left[\left.\frac{\partial K_A}{\partial A}\right|_A \frac{F_1}{\sin\vartheta} + K_A\Big|_A\left(\frac{2F_1}{\bar{b}\sin\vartheta} + F_2\right)\right] \tag{30b}$$

with

$$F_1 = \int_0^1 \bar{\eta}\sqrt{1-\bar{\eta}^2}\, K_{\bar{h}}\Big|_{\bar{\eta}}\, d\bar{\eta}$$

$$F_2 = \int_0^1 \bar{\eta}^2\sqrt{1-\bar{\eta}^2}\, \frac{\partial K_{\bar{h}}}{\partial \bar{h}}\Big|_{\bar{\eta}}\, d\bar{\eta}\,.$$

Together with the stabilizing moment a lateral force is effective, the magnitude of which is

$$dP_y = \frac{\partial P_y}{\partial A}\, dA + \frac{\partial P_y}{\partial \bar{b}}\, d\bar{b} + \frac{\partial P_y}{\partial \bar{h}}\, d\bar{h}\,. \tag{31}$$

The general term for the lateral force is given by

$$P_y\Big|_{A_1\bar{b}_1\bar{h}_2} = \rho u_0^2 b c\; C_{L\infty} K_\alpha K_P \sin\vartheta\; K_A\Big|_A \frac{4}{\pi}\int_0^1 \sqrt{1-\bar{\eta}^2}\, K_{\bar{h}}\Big|_{\bar{\eta}}\, d\bar{\eta}\,. \tag{32}$$

With the differentials

$$dA = \mp\, d\beta\, \frac{\bar{b}}{\tan\vartheta} = d\bar{b}$$

$$d\bar{h} = \mp\, d\beta\; \bar{b}\; \bar{\eta}\, \cos\vartheta$$

and

$$\frac{\partial P_y}{\partial A}\Big|_{A_1\bar{b}_1\bar{h}_2} = \frac{1}{2}\rho u_0^2 bc\; C_{L\infty} K_\alpha K_P \sin\vartheta\; \frac{\partial K_A}{\partial A}\Big|_A \frac{4}{\pi}\int_0^1 \sqrt{1-\bar{\eta}^2}\, K_{\bar{h}}\Big|_{\bar{\eta}}\, d\bar{\eta} \tag{33a}$$

$$\frac{\partial P_y}{\partial \bar{b}}\Big|_{A_1\bar{b}_1\bar{h}_2} = \frac{1}{2}\rho u_0^2 bc\; C_{L\infty} K_\alpha K_P \sin\vartheta\; \frac{1}{\bar{b}} K_A\Big|_A \frac{4}{\pi}\int_0^1 \sqrt{1-\bar{\eta}^2}\, K_{\bar{h}}\Big|_{\bar{\eta}}\, d\bar{\eta} \tag{33b}$$

$$\frac{\partial P_y}{\partial \bar{h}}\Big|_{A_1\bar{b}_1\bar{h}_2} = \frac{1}{2}\rho u_0^2 bc\; C_{L\infty} K_\alpha K_P \sin\vartheta\; K_A\Big|_A \frac{4}{\pi}\int_0^1 \sqrt{1-\bar{\eta}^2}\, \frac{\partial K_{\bar{h}}}{\partial \bar{h}}\Big|_{\bar{\eta}}\, d\bar{\eta}, \tag{33c}$$

the resulting change of lateral force is found to be

$$\left.\frac{dP_y}{d\beta}\right|_{A,\bar{b},\bar{h}_2} = \rho u_0^2\, bc\, C_{L\infty} K_\alpha K_P \cos\vartheta\, \bar{b} \left[\left.\frac{\partial K_A}{\partial A}\right|_A \left. K_{\bar{h}_m} \right|_{\bar{h}_2} + \left. K_A \right|_A \left(\frac{1}{\bar{b}} \left. K_{\bar{h}_m} \right|_{\bar{h}_2} + \frac{4}{\pi} \sin\vartheta\, F_3 \right) \right] \tag{34a}$$

and

$$\left.\frac{dC_{P_y}}{d\beta}\right|_{A,\bar{b},\bar{h}_2} = C_{L\infty} K_\alpha K_P \cos\vartheta\, \bar{b} \left[\left.\frac{\partial K_A}{\partial A}\right|_A \left. K_{\bar{h}_m} \right|_{\bar{h}_2} + \left. K_A \right|_A \left(\frac{1}{\bar{b}} \left. K_{\bar{h}_m} \right|_{\bar{h}_2} + \frac{4}{\pi} \sin\vartheta\, F_3 \right) \right] \tag{34b}$$

with

$$F_3 = \int_0^1 \bar{\eta} \sqrt{1 - \bar{\eta}^2} \left.\frac{\partial K_{\bar{h}}}{\partial \bar{h}}\right|_{\bar{\eta}} d\bar{\eta} .$$

Using the terms $dC_{M_x}/d\beta$ and $dC_{P_y}/d\beta$ the position of the initial lateral metacenter above lowest point can be found [7]:

$$z_0 = -C \frac{dC_{M_x}}{d\beta} \left. \frac{1}{C_L + \frac{dC_{P_y}}{dy}} \right|_{\beta=0} . \tag{35}$$

Analogously, stabilizing moment and lateral force for any inclination β can be found. The different values K_A and dK_A/dA have to be taken [7] considering the wetted breadth for both panels relative to the profile length. In addition to that a dependence on β appears, i.e., for the moment there has to be written:

$$dM_x = \frac{\partial M_x}{\partial A} dA + \frac{\partial M_x}{\partial \bar{b}} d\bar{b} + \frac{\partial M_x}{\partial \bar{h}} d\bar{h} + \frac{\partial M_x}{\partial \beta} d\beta.$$

For the case of the submerged dihedral foil as well as of a submerged flat foil all the terms taking care of the change of the aspect ratio and of the breadth will disappear. The rolling stability of submerged foils therefore is principally less than that of dihedral foils piercing the surface.

As in the case of vertical stabilization, a lateral stabilization might be possible for submerged foils as well if the depth of submergence is low or if horizontal stabilizing plates are arranged near the free surface.

For a submerged dihedral foil the lowest point of which is running at the depth $\bar{h}_2$ with the upper ends at the depth $\bar{h}_1$ the gradient of the rolling moment in the upright position becomes

$$\left.\frac{dC_{M_x}}{d\beta}\right|_{A_1\bar{b}_1\bar{h}_1,\bar{h}_2} = -C_{L\infty}K_\alpha K_P \cos\vartheta\ \bar{b}^2 \frac{4}{\pi} K_A\Big|_A \int_0^1 \bar{\eta}^2\sqrt{1-\bar{\eta}^2}\left.\frac{dK_{\bar{h}}}{d\bar{h}}\right|_{\bar{\eta}} d\bar{\eta} \tag{36}$$

and the gradient of the lateral force becomes

$$\left.\frac{dC_{P_y}}{d\beta}\right|_{A_1\bar{b}_1\bar{h}_1,\bar{h}_2} = C_{L\infty}K_\alpha K_P \cos\vartheta\ \sin\vartheta\, \bar{b}\frac{4}{\pi} K_A\Big|_A \int_0^1 \bar{\eta}\sqrt{1-\bar{\eta}^2}\left.\frac{dK_{\bar{h}}}{d\bar{h}}\right|_{\bar{\eta}} d\bar{\eta} \tag{37}$$

with

$$\bar{h}_1 \le \bar{h}(\bar{\eta}) \le \bar{h}_2 .$$

For a parallel submerged foil running at the depth $\bar{h}_0$,

$$\left.\frac{dC_{M_x}}{d\beta}\right|_{A_1\bar{b}_1\bar{h}_0} = -C_{L\infty}K_P\bar{b}^2\frac{4}{\pi}K_A\Big|_A \left.\frac{dK_{\bar{h}}}{d\bar{h}}\right|_{\bar{h}_0}\int_0^1 \bar{\eta}^2\sqrt{1-\bar{\eta}^2}\,d\bar{\eta}$$

$$= -C_{L\infty}K_P\bar{b}^2\frac{1}{4}K_A\Big|_A \left.\frac{dK_{\bar{h}}}{d\bar{h}}\right|_{\bar{h}_0} \tag{38}$$

and

$$\left.\frac{dC_{P_y}}{d\beta}\right|_{A_1\bar{b}_1\bar{h}_0} = 0 \qquad (dA = d\bar{b} = 0). \tag{39}$$

The lateral stabilization due to sideslipping will not be developed here since this can be done in a manner corresponding to the treatment of the vertical and of the rolling stability.

NOMENCLATURE

b	semispan of the hydrofoil
$b_{proj} = b\cos\vartheta$	
c	chord length
$\bar{b} = b/c$	

h	depth of submergence of the foil
h'	minimum local water depth above the foil
$\bar{h} = h/c$	
$h^* = h/(c/2)$	
$A = 2b/c$	aspect ratio
$S = 2bc$	area of the hydrofoil
u_0	running speed
u_1	induced velocity in the direction of the undisturbed flow
w_1	induced velocity perpendicular to the direction of the undisturbed flow
$F_h = u_0/\sqrt{gh}$	Froude depth number
α_{geom}	geometrical angle of attack of the chord
α_0	no-lift angle
m	camber
$C_L = L/\rho u_0^2 bc$	lift coefficient
C_D	drag-coefficient
C_P	transverse-force coefficient
$C_{M_x} = M_x/\rho u_0^2 bc^2$	rolling-moment coefficient
ϑ	dihedral angle
β	rolling angle
γ	sideslip angle
$\varepsilon = C_D/C_L$	drag-lift ratio

REFERENCES

[1] Laitone, E.V., "Limiting Pressure on Hydrofoils at Small Submergence Depths," J. Appl. Phys. 25:623 (1954)

[2] Parkin, B.R., Perry, B., and Wu, Y.T., "Pressure Distribution on a Hydrofoil Running Near the Water Surface," J. Appl. Phys. 27:232 (1956)

[3] Plesset, M.S., and Parkin, B.R., "Hydrofoils in Noncavitating and Cavitating Flow," Cavitation in Hydrodynamics, Nat. Phys. Lab., 1955

[4] Land, N.S., "Characteristics of an NACA 66, S-209 Section Hydrofoil at Several Depths," NACA W.R.L.-757, 1943

[5] Schuster, S., and Schwanecke, H., "Über den Einfluss der Wasseroberfläche auf die Auftriebsverteilung von Tragflügeln," Schiffstechnik 4:117 (1957)

[6] Schuster, S., and Logothetopoulos, J., "Sechskomponentenmessungen an einer Wassertragfläche zur Untersuchung der Einflüsse von Streckung, Kielung und Krängung," Versuchs-Abtlg. d. Gebr. Sachsenberg AG. No. 5a, 1942 (unpublished)

[7] Schwanecke, H., "Über Sechskomponenten-Messungen an einem V-Wassertragflügel bei symmetrischer und unsymmetrischer Anströmung," Schiffstechnik 6:93 (1957)

[8] Isay, W.H., "Zur Theorie der nahe der Wasseroberfläche fahrenden Tragflächen," Ingenieur-Archiv 27:295 (1959/60)

[9] Weinig, F., "Beitrag zur Theorie des Tragflügels endlicher, insbesondere kleiner Spannweite," Luftfahrt-Forschung 13:405 (1936)

DISCUSSION

P. Kaplan (Technical Research Group, Inc., Syosset, New York)

I noticed, or it appeared to me, that the influence of roll was only static. I wonder if you have considered or done any work, not reported here, as to the effect of the roll damping, that is, what happens when the foil is performing not just a static roll, deflection, but is actually performing a roll angular motion? This is important since it is the roll damping that determines the major behavior of the roll motion. According to the results of the free motion studies, there was quite different behavior of the system as compared to an aircraft, so I wonder just what influence a dihedral will have on the roll damping and if any consideration was given to this problem.

S. Schuster

Our results given here of the tests and formulas are valid only for the steady state. Even the test for finding the point of breaking down of the lift shows only the beginning of the motion. Damping forces and moments can only be found during the motion itself. We are beginning the investigation for the unsteady problems, especially for hydrofoils in waves, but at present we are not able to give you an answer to these special questions. I think that damping is higher for rolling than for yawing, but for the whole system of two or more hydrofoils, we have to consider sideslip motion too. Perhaps there will be something to report after finishing our investigations on oscillations of a propeller in the axial direction and in the rotational direction.

* * *